Supplementary Information

Redox-Based Defect Detection in Packed DNA: Insights from Hybrid Quantum Mechanical/Molecular Mechanics Molecular Dynamics Simulations

Murat Kılıç[†], Polydefkis Diamantis[†], Sophia K. Johnson, Oliver Toth, and Ursula Rothlisberger[*]

Laboratory of Computational Chemistry and Biochemistry, Institute of Chemical Sciences and Engineering, École Polytechnique Fédérale de Lausanne (EPFL), CH-1015 Lausanne, Switzerland

E-mail: ursula.roethlisberger@epfl.ch

Discussion on accounting for the finite size of the periodic simulation box:
In the literature, a set of corrections concerning the effects of a finite simulation box on redox calculations has been outlined (reference 63). First, the calculated reorganization energy lacks contributions from higher order solvation shell changes due to finite volume of the simulation box. First, the calculated reorganization energy lacks contributions from higher order solvation shell changes due to finite volume of the simulation box. To reduce errors in the reorganization energy, corrections must be explicitly added and/or the simulated system must be solvated well enough to mimic an "infinitely diluted" system. The current study utilizes a large simulation box (dimensions of 148 Å × 159 Å × 107 Å).

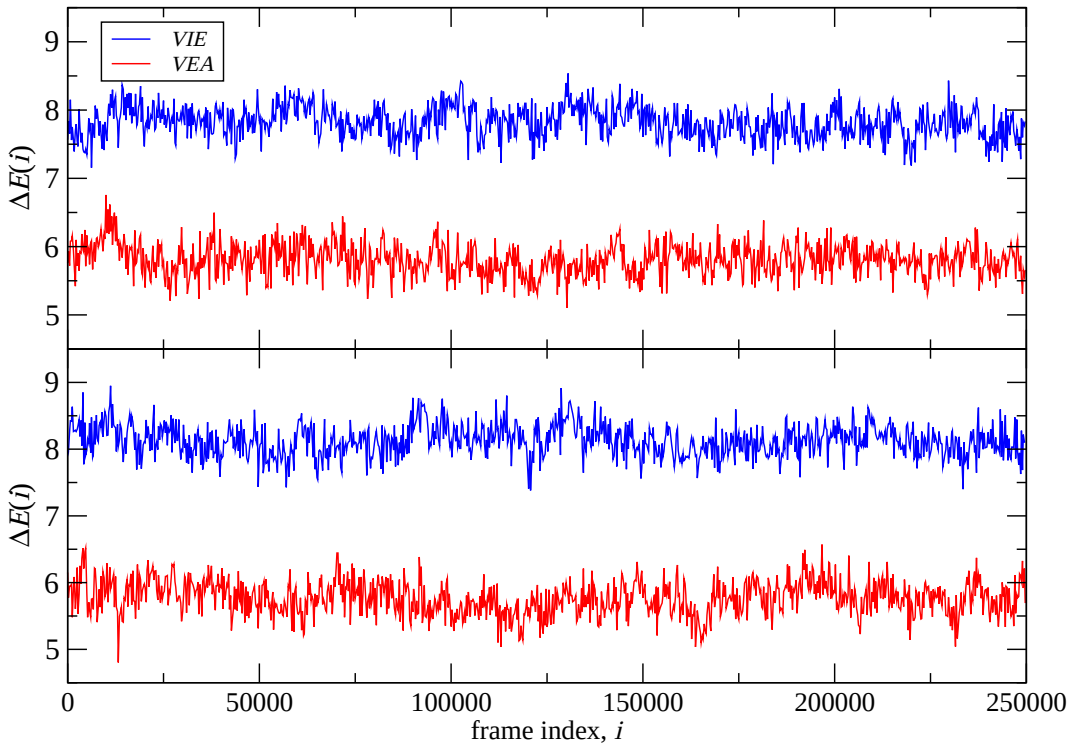

Figure 1: Time series of the vertical ionization energies (*VIE*s) and vertical electron affinities (*VEA*s) used for the determination of the vertical energy gap distributions and redox properties of the native G-rich **regions 1** (**top**) and **2** (**bottom**).

Additionally, the system is thoroughly solvated with approximately 76500 water molecules. Together, this simulation box mimics an "infinitely diluted" system which mitigates the need for explicitly added corrections.

Second, charge neutrality must be enforced for the accurate calculation of redox properties. Without guaranteed charge neutrality, a correction term must be included when calculating reorganization energy values. The charge neutrality of the current study's simulation box is maintained through the explicit inclusion of sodium and chloride counterions which maintain an overall system charge of zero. Therefore, a correction term to account for differences across systems when calculating redox properties in this study is not necessary.

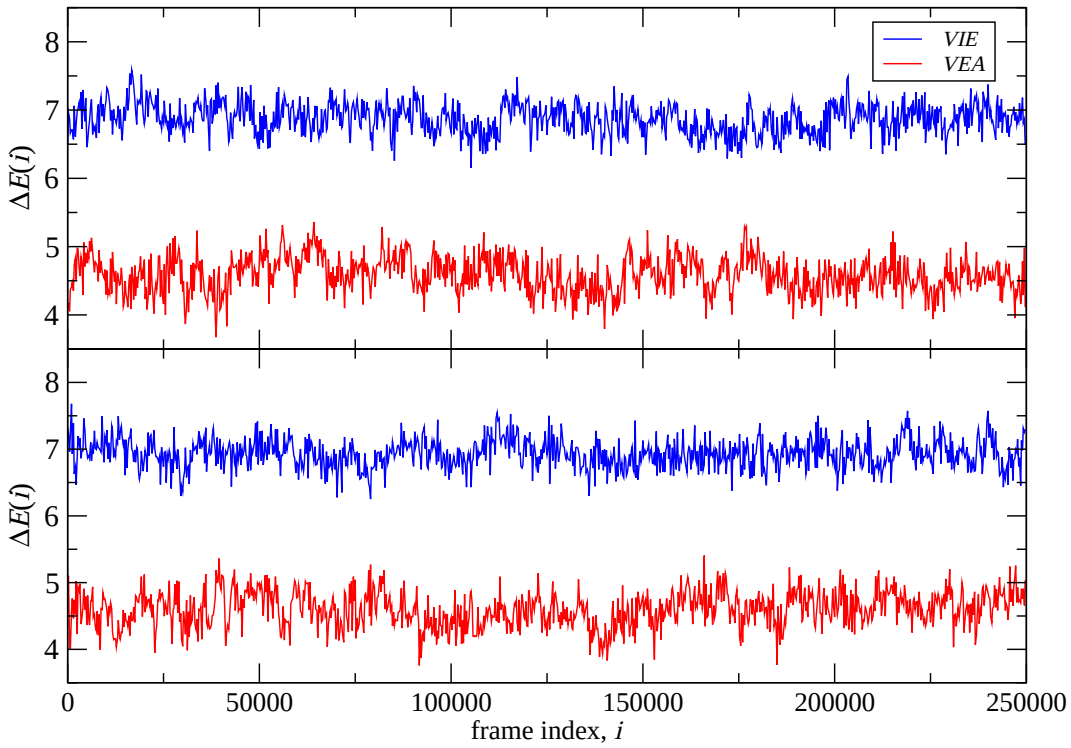

Figure 2: Time series of the *VIE*s and *VEA*s used for the determination of the vertical energy gap distributions and redox properties of the defect systems in which the 8-oxoguanine (8oxoG) base was placed in G-rich **regions 1** (**top**) and **2** (**bottom**).

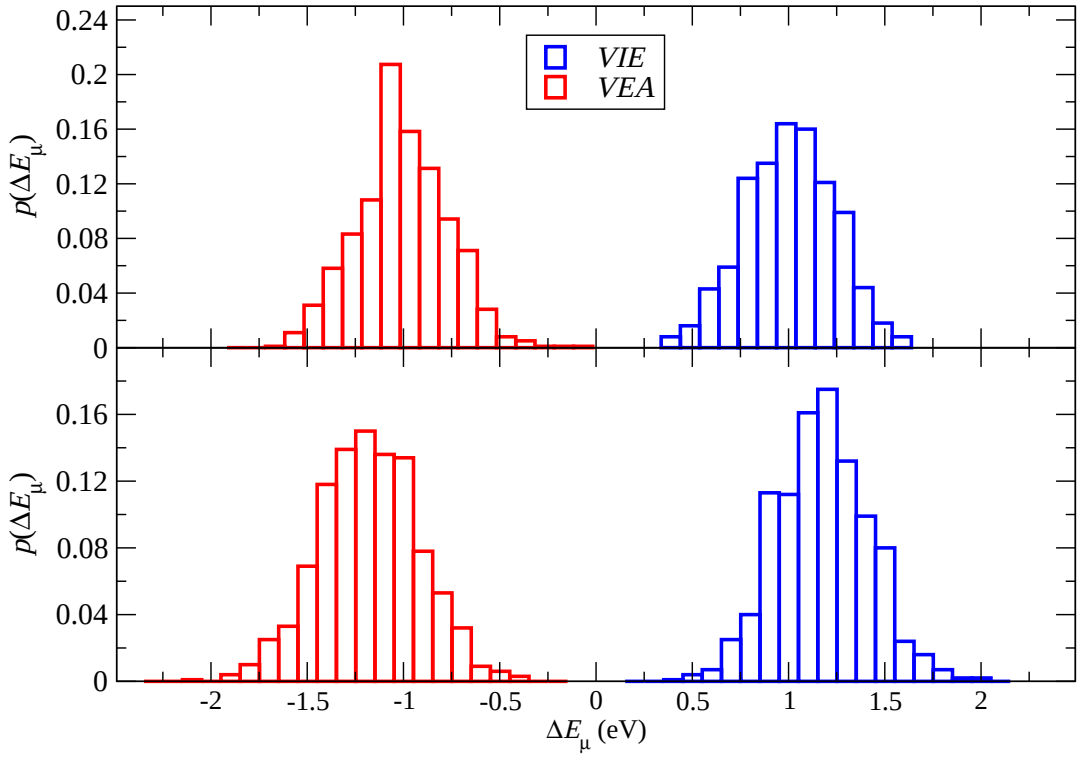

Figure 3: *VIE* and *VEA* distributions for the native G-rich **regions 1** (**top**) and **2** (**bottom**).

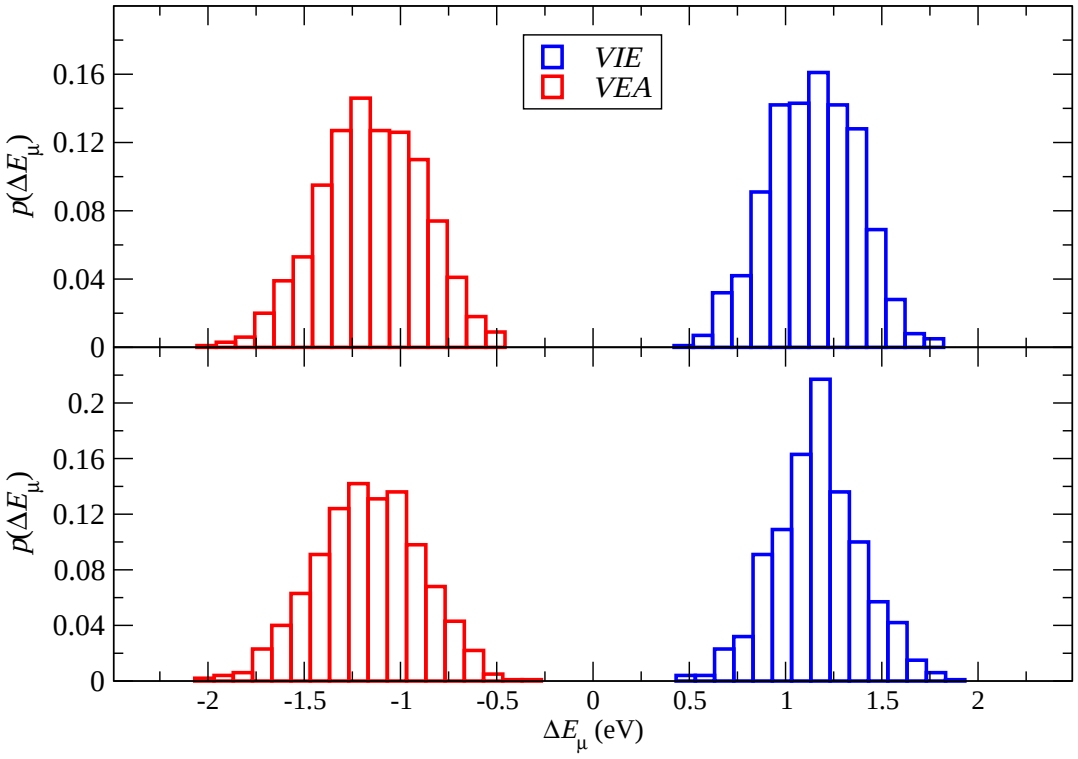

Figure 4: *VIE* and *VEA* distributions for the defect systems in which 8oxoG was placed in in G-rich **regions 1** (**top**) and **2** (**bottom**).

5' - ATCAATATCCACCTGCAGATTCTACCAAAAGTGTATTTGGAAACTGCTCCATCAAAAG**G***CATGTTCAGCTGAA
TTCAGCTGAACATGCCTTTTGATGGAGCAGTTTCCAAATACACTTTTGGTAGAATCTGCAGGTGGATATTGAT - 3'

Figure 5: DNA sequence of strand 1, with the guanine marked at base 59 corresponding to the central base of **region 1**. Strand 2 has the same sequence in the 3' to 5' direction as strand 1 in the 5' to 3' direction. On strand 2 **region 2** has a central base at a reciprocal location to region 1.

Table 1: G-rich **region 1** systems: Root mean square fluctuations (RMSFs) for the DNA residues belonging in the QM region of the native (left) and 8oxoG-containing (right) systems.

Native				8oxoG			
Reduced		Oxidized		Reduced		Oxidized	
ResID	RMSF (Å)	ResID	RMSF (Å)	ResID	RMSF (Å)	ResID	RMSF (Å)
58	0.46	58	0.47	58	0.43	58	0.44
59	0.44	59	0.40	59	0.46	59	0.39
60	0.43	60	0.40	60	0.48	60	0.41
233	0.58	233	0.45	233	0.47	233	0.43
234	0.55	234	0.40	234	0.50	234	0.61
235	0.51	235	0.61	235	0.63	235	0.54

Table 2: G-rich **region 2** systems: Root mean square fluctuations (RMSFs) for the DNA residues belonging in the QM region of the native (left) and 8oxoG-containing (right) systems.

Native				8oxoG			
Reduced		Oxidized		Reduced		Oxidized	
ResID	RMSF (Å)	ResID	RMSF (Å)	ResID	RMSF (Å)	ResID	RMSF (Å)
87	0.52	87	0.58	87	0.46	87	0.49
88	0.48	88	0.48	88	0.42	88	0.40
89	0.53	89	0.48	89	0.44	89	0.39
204	0.67	204	0.45	204	0.42	204	0.50
205	0.44	205	0.45	205	0.38	205	0.44
206	0.56	206	0.44	206	0.43	206	0.48

Table 3: G-rich **region 1** systems: QM-treated DNA and neighboring protein residues sharing a strong intermolecular interaction in the native (left) and 8oxoG-containing (right) systems.

Native				8oxoG			
Reduced		Oxidized		Reduced		Oxidized	
ResID_{DNA}	$\text{ResID}_{Pro.}$	ResID_{DNA}	$\text{ResID}_{Pro.}$	ResID_{DNA}	$\text{ResID}_{Pro.}$	ResID_{DNA}	$\text{ResID}_{Pro.}$
58	–	58	–	58	–	58	–
59	–	59	–	59	–	59	318
60	407	60	401 / 407	60	318 / 401	60	318 / 407
233	–	233	–	233	–	233	–
234	–	234	–	234	–	234	–
235	391	235	–	235	–	235	–

Table 4: G-rich **region 2** systems: QM-treated DNA and neighboring protein residues sharing an intermolecular interaction in the native (left) and 8oxoG-containing (right) systems. With the exception of a strong (206-731) and a weak (204-688) interaction found for for the oxidized native system, no intermolecular interactions were identified.

Native				8oxoG			
Reduced		Oxidized		Reduced		Oxidized	
ResID_{DNA}	$\text{ResID}_{Pro.}$	ResID_{DNA}	$\text{ResID}_{Pro.}$	ResID_{DNA}	$\text{ResID}_{Pro.}$	ResID_{DNA}	$\text{ResID}_{Pro.}$
87	–	87	–	87	–	87	–
88	–	88	–	88	–	88	–
89	–	89	–	89	–	89	–
204	–	204	688	204	–	204	–
205	–	205	–	205	–	205	–
206	–	206	731	206	–	206	–

Table 5: The 3 DNA base pairs which comprise the G-rich **region 2** systems have a greater number of average H-bonding interactions with solvent molecules throughout the classical molecular dynamics simulation than the 3 DNA base pairs of the G-rich **region 1** systems indicating that **region 2** is more solvent-exposed than **region 1** regardless of the presence or absence of the 8oxoguanine defect. Average H-bonding interactions between the DNA bases and solvent molecules were calculated with GROMACS hydrogen bonding tool with counts viable hydrogen bonding interactions throughout a trajectory for selected donor and acceptor groups.

Native		8oxoG	
Region 1	Region 2	Region 1	Region 2
46.70	53.65	50.87	54.38

Table 6: The central guanine or 8oxoguanine which comprises the G-rich **region 2** systems have a greater number of average H-bonding eligible solvent partners within 0.35nm throughout the classical molecular dynamics simulation than the central guanine or 8oxoguanine of the G-rich **region 1** systems indicating that **region 2** is more solvent-exposed than **region 1** even on the central base level. Average H-bonding eligible partners between the DNA base and solvent molecules were calculated with GROMACS hydrogen bonding tool with counts viable hydrogen bonding partners within 0.35nm throughout a trajectory for selected donor and acceptor groups.

Native		8oxoG	
Region 1	Region 2	Region 1	Region 2
6.93	10.20	9.66	11.36

Table 7: Average number of oxygen solvent atoms within 3.5 Åof the N7 atom on the central base of the quantum region (guanine or 8oxoguanine) throughout the entire QM/MM MD trajectory. Local changes of the reduced versus oxidized base in terms of nearby solvent coordination is very low.

Native				8oxoG			
Region 1		Region 2		Region 1		Region 2	
Red	Ox	Red	Ox	Red	Ox	Red	Ox
1.6 ± 0.75	1.9 ± 0.65	2.1 ± 0.66	2.0 ± 0.73	2.0 ± 0.79	2.1 ± 0.83	2.1 ± 0.81	2.1 ± 0.78

Table 8: Means and standard deviations of DNA structural parameters.

	Parameter	Wild-Type	Region 1 Defect	Region 2 Defect
Intrabase	Shear	-0.017 ± 0.0375	-0.0049 ± 0.03335	-0.0045 ± 0.03251
Translational	Stretch	0.024 ± 0.0133	0.026 ± 0.0137	0.032 ± 0.0143
(Å)	Stagger	0.062 ± 0.0491	0.045 ± 0.0486	0.028 ± 0.0494
Intrabase	Buckle	-0.25 ± 1.181	-0.92 ± 1.186	-0.48 ± 1.215
Rotational	Propeller	-9.4 ± 0.86	-9.1 ± 0.81	-9.5 ± 0.78
(°)	Opening	1.5 ± 0.50	1.3 ± 0.53	1.2 ± 0.51
Interbase	Shift	-0.0089 ± 0.03612	0.0051 ± 0.04081	-0.0073 ± 0.03876
Translational	Slide	-0.25 ± 0.048	-0.25 ± 0.048	-0.25 ± 0.053
(Å)	Rise	3.39 ± 0.011	3.38 ± 0.012	3.39 ± 0.013
Interbase	Tilt	0.014 ± 0.2473	0.031 ± 0.2664	0.033 ± 0.2608
Rotational	Roll	-0.27 ± 0.354	-0.26 ± 0.400	-0.055 ± 0.3771
(°)	Twist	34.5 ± 0.10	34.4 ± 0.13	34.6 ± 0.12
Base-Axis	XDisp	-0.41 ± 0.059	-0.44 ± 0.064	-0.48 ± 0.066
Translational (Å)	YDisp	0.014 ± 0.0456	-0.0062 ± 0.05056	0.015 ± 0.0499
Base-Axis	Inclination	-0.22 ± 0.577	-0.12 ± 0.656	0.23 ± 0.618
Rotational (°)	Tip	-0.063 ± 0.4044	-0.057 ± 0.442	-0.12 ± 0.430
Strand 1	Alpha1	-70. ± 2.3	-69 ± 2.4	-70. ± 2.0
Torsional Angles	Beta1	76 ± 12.9	74 ± 12.4	80 ± 12.8
(°)	Gamma1	53 ± 3.7	51 ± 4.6	55 ± 2.5
	Delta1	136 ± 1.2	136 ± 1.4	133 ± 1.3
	Epsilon1	-92 ± 11.8	-96 ± 11.4	-86 ± 11.9
	Zeta1	-53 ± 6.4	-55 ± 7.3	-56 ± 6.7
	Chi1	-113 ± 1.5	-113 ± 1.7	-113 ± 1.6
Strand 2	Alpha2	-72 ± 2.1	-70. ± 2.2	-71 ± 2.1
Torsional Angles	Beta2	80. ± 12.5	78 ± 13.3	77 ± 12.7
(°)	Gamma2	51 ± 4.0	52 ± 3.6	53 ± 3.2
	Delta2	136 ± 1.2	136 ± 1.3	134 ± 1.3
	Epsilon2	-96 ± 11.5	-92 ± 12.2	-88 ± 11.8
	Zeta2	-51 ± 6.7	-55 ± 7.4	-56 ± 6.7
	Chi2	-112 ± 1.5	-112 ± 1.4	-112 ± 1.5
Strand 1	Phase1	117 ± 8.2	120. ± 8.2	117 ± 8.3
Sugar Pucker (°)	Amplitude1	41.1 ± 0.49	41.2 ± 0.50	41.0 ± 0.51
Strand 2	Phase2	117 ± 8.7	116 ± 8.2	118 ± 8.3
Sugar Pucker (°)	Amplitude2	41.4 ± 0.19	41.2 ± 0.53	41.2 ± 0.51
Helical Axis	H-Rise	3.36 ± 0.017	3.37 ± 0.020	3.34 ± 0.021
(Å; °)	H-Twist	35.30 ± 0.093	35.3 ± 0.12	35.5 ± 0.11
	Ax-Bend	4.93 ± 0.082	4.89 ± 0.083	4.90 ± 0.088
Minor	Minor W	5.1 ± 0.12	5.1 ± 0.15	5.3 ± 0.12
Groove (Å)	Minor D	5.26 ± 0.044	5.25 ± 0.044	5.21 ± 0.050
Major	Major W	11.5 ± 0.13	11.6 ± 0.15	11.5 ± 0.14
Groove (Å)	Major D	4.7 ± 0.13	4.8 ± 0.15	4.8 ± 0.14

Table 9: Z-scores for selected parameters whose difference in mean falls outside one or both of the individual distribution standard deviations.

Parameter	Z-Score
Twist Reg2	0.64
XDisp Reg2	0.79
Inclin. Reg2	0.61
Delta1 Reg2	1.4
Delta2 Reg2	1.1
H-Twi Reg2	1.4
Min.W Reg2	1.2
Maj.W R1	0.50
Maj.D R1	0.50
Maj.D R2	0.52

Table 10: Means and standard deviations of selected DNA structural parameters by section. Selected parameters exhibit differences in wild-type and defect mean greater than the associated distribution widths (standard deviations).

Parameter	Section 1	Section 2	Section 3	Section 4
Twist (°)				
WT	35.3 ± 0.42	34.7 ± 0.44	34.3 ± 0.35	34.8 ± 0.36
R2 Defect	35.8 ± 0.44	34.7 ± 0.42	34.6 ± 0.34	35.1 ± 0.41
XDisp (Å)				
WT	-0.19 ± 0.145	-0.21 ± 0.142	-0.39 ± 0.137	-0.283 ± 0.145
R2 Defect	-0.059 ± 0.1431	-0.44 ± 0.145	-0.41 ± 0.152	-0.27 ± 0.158
Inclin. (°)				
WT	-1.4 ± 1.35	-3.0 ± 1.36	-0.53 ± 1.522	-1.7 ± 1.35
R2 Defect	-0.83 ± 1.353	-3.0 ± 1.45	0.67 ± 1.334	-1.2 ± 1.29
Delta1 (°)				
WT	136 ± 2.6	137 ± 2.8	134 ± 3.1	137 ± 2.8
R2 Defect	136 ± 2.7	134 ± 3.4	132 ± 3.4	135 ± 3.0
Delta2 (°)				
WT	137 ± 2.7	138 ± 2.5	136 ± 3.2	137 ± 2.7
R2 Defect	137 ± 3.1	134 ± 2.8	133 ± 3.4	135 ± 3.1
H-Twi (°)				
WT	35.9 ± 0.40	35.7 ± 0.40	35.2 ± 0.33	35.5 ± 0.35
R2 Defect	36.4 ± 0.39	35.7 ± 0.38	35.5 ± 0.33	35.7 ± 0.39
Min.W (Å)				
WT	5.1 ± 0.23	4.8 ± 0.25	5.1 ± 0.27	5.1 ± 0.26
R2 Defect	5.1 ± 0.27	5.1 ± 0.28	5.4 ± 0.30	5.2 ± 0.28
Maj.W (Å)				
WT	11.1 ± 0.30	11.4 ± 0.27	11.5 ± 0.29	11.6 ± 0.29
R1 Defect	11.3 ± 0.30	11.5 ± 0.29	11.3 ± 0.28	11.8 ± 0.33
Maj.D (Å)				
WT	4.6 ± 0.29	4.5 ± 0.31	4.7 ± 0.28	4.6 ± 0.28
R1 Defect	4.3 ± 0.29	4.5 ± 0.32	5.0 ± 0.28	4.7 ± 0.27
R2 Defect	4.5 ± 0.27	4.7 ± 0.31	4.8 ± 0.28	4.5 ± 0.30

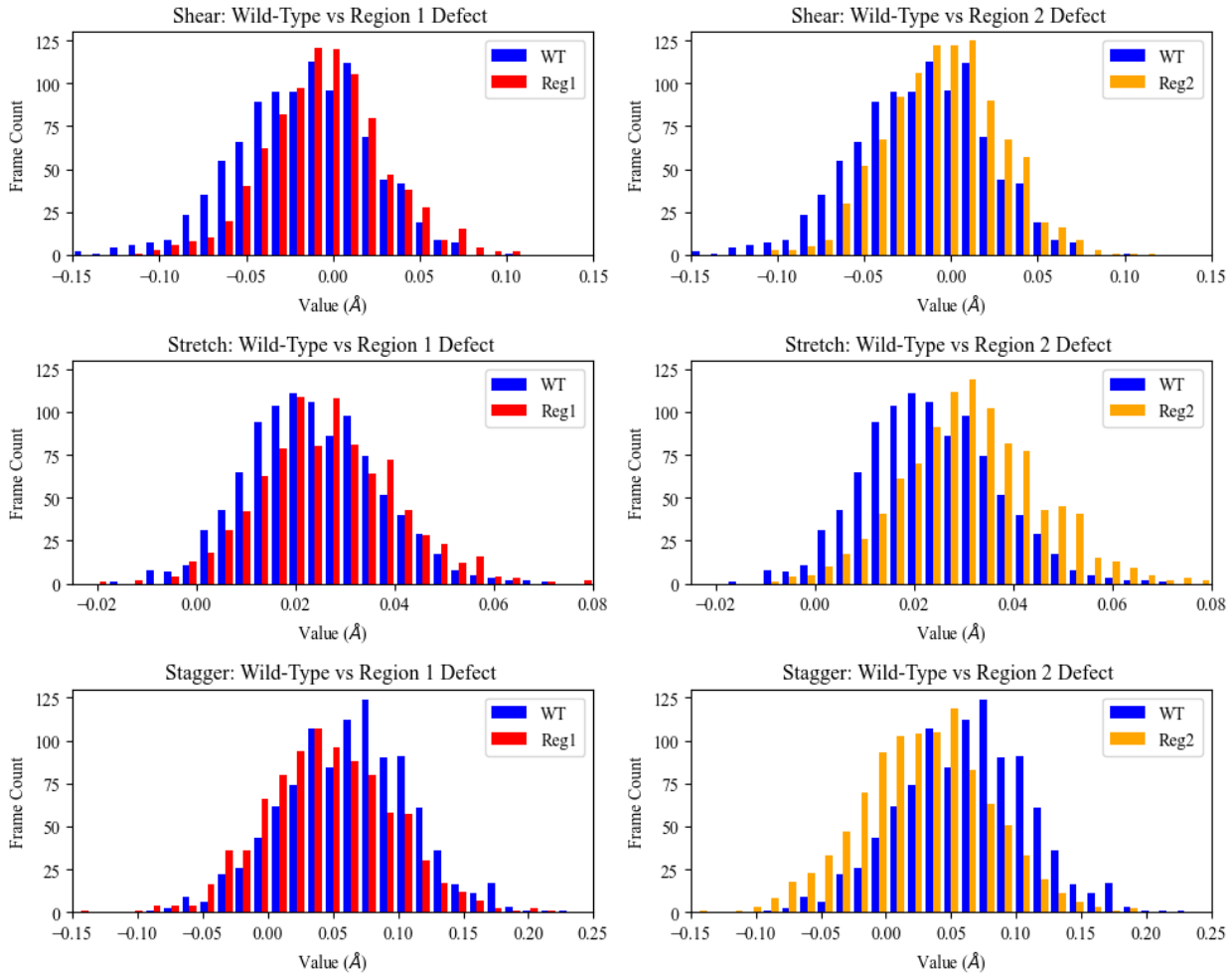

Figure 6: Population distributions of intrabase translational parameters (shear, stretch, and stagger) for wild-type system (WT, blue) vs region 1 defect system (Reg1, red) and for wild-type system (WT, blue) vs region 2 defect system (Reg2, orange). The systems do not include in their analysis the 40 base pairs associated with tail regions.

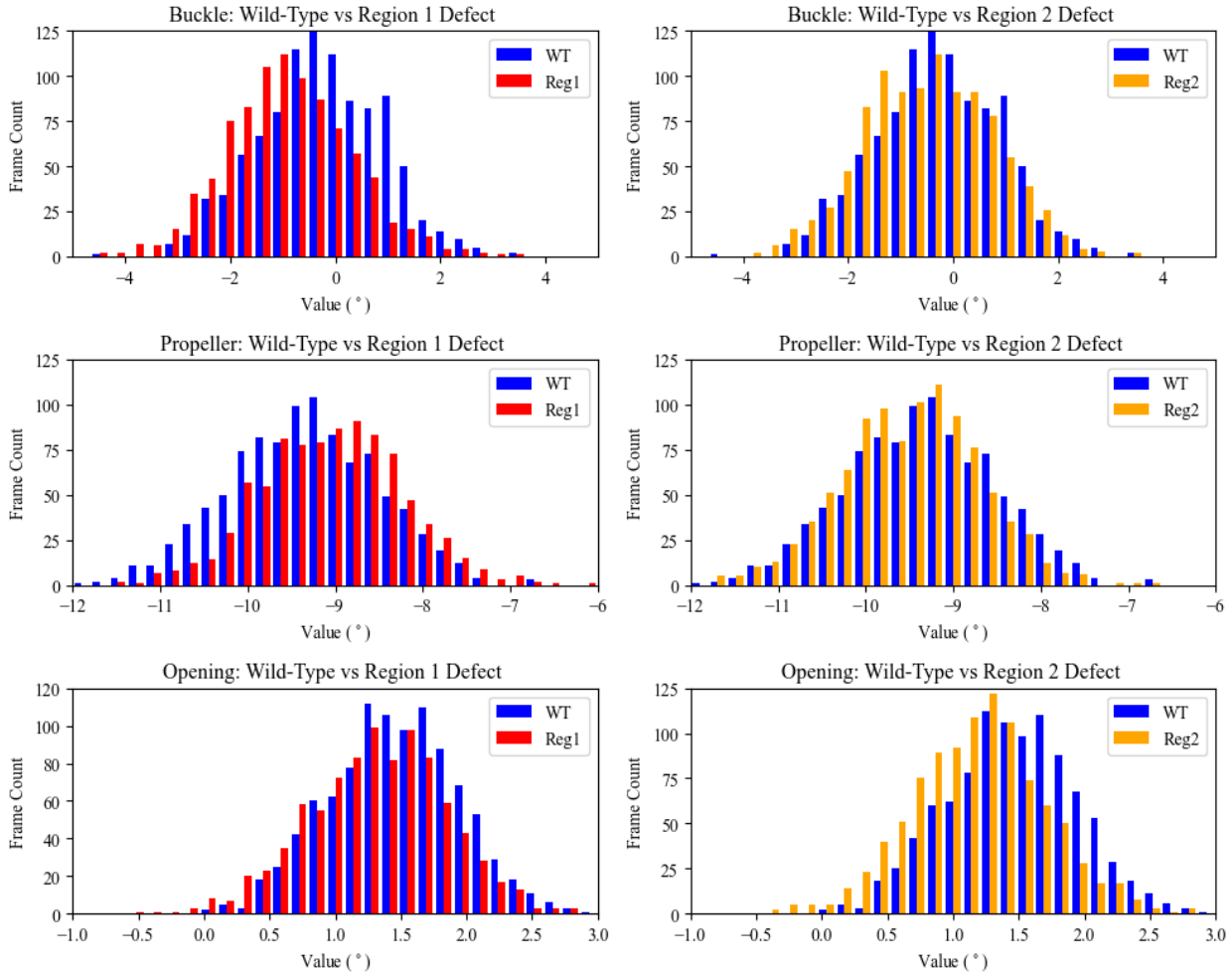

Figure 7: Population distributions of intrabase rotational parameters (buckle, propeller, and opening) for wild-type system (WT, blue) vs region 1 defect system (Reg1, red) and for wild-type (WT, blue) vs region 2 defect system (Reg2, orange). The systems do not include in their analysis the 40 base pairs associated with tail regions.

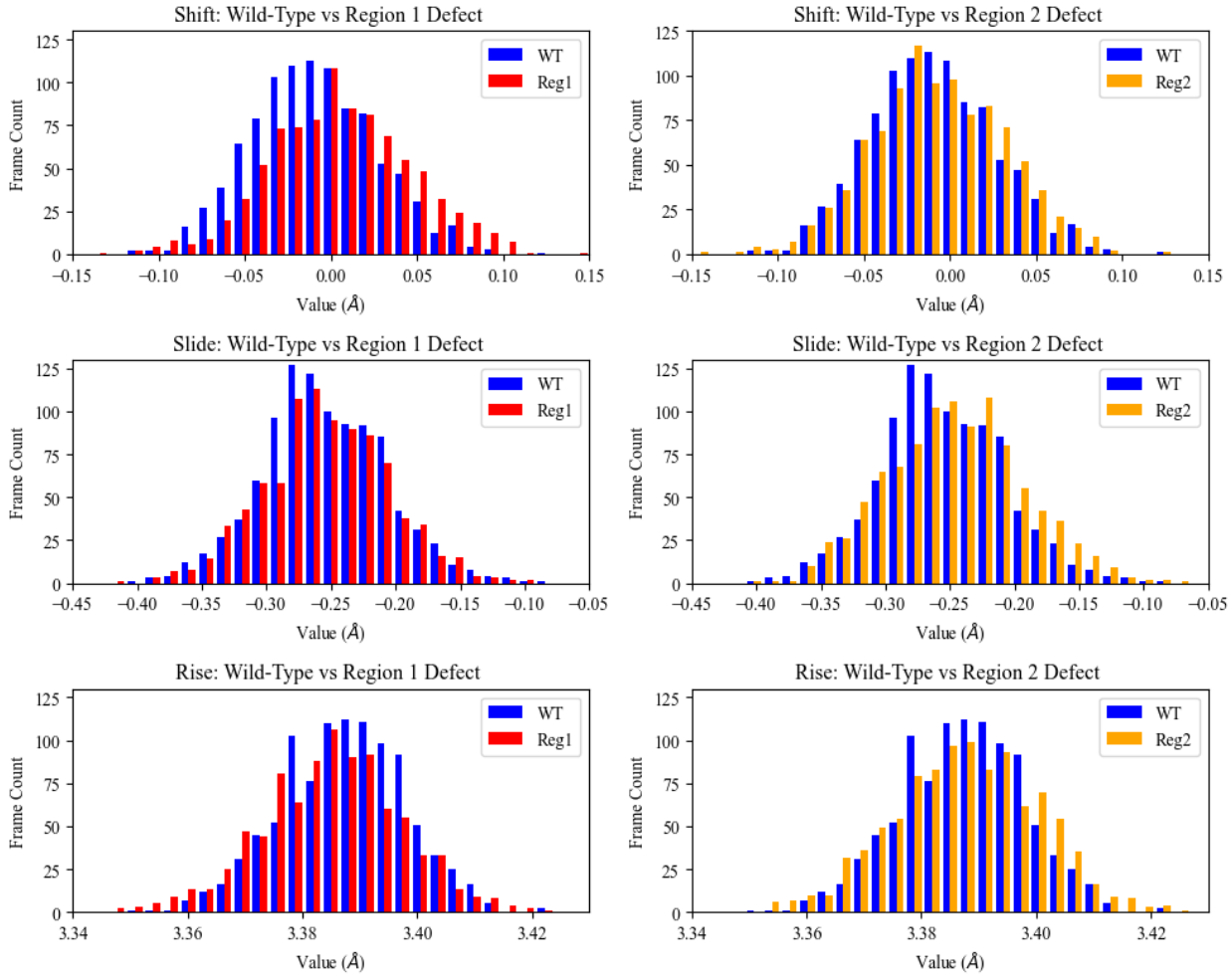

Figure 8: Population distributions of interbase translational parameters (shift, slide, and rise) for wild-type system (WT, blue) vs region 1 defect system (Reg1, red) and for wild-type system (WT, blue) vs region 2 defect system (Reg2, orange). The systems do not include in their analysis the 40 base pairs associated with tail regions.

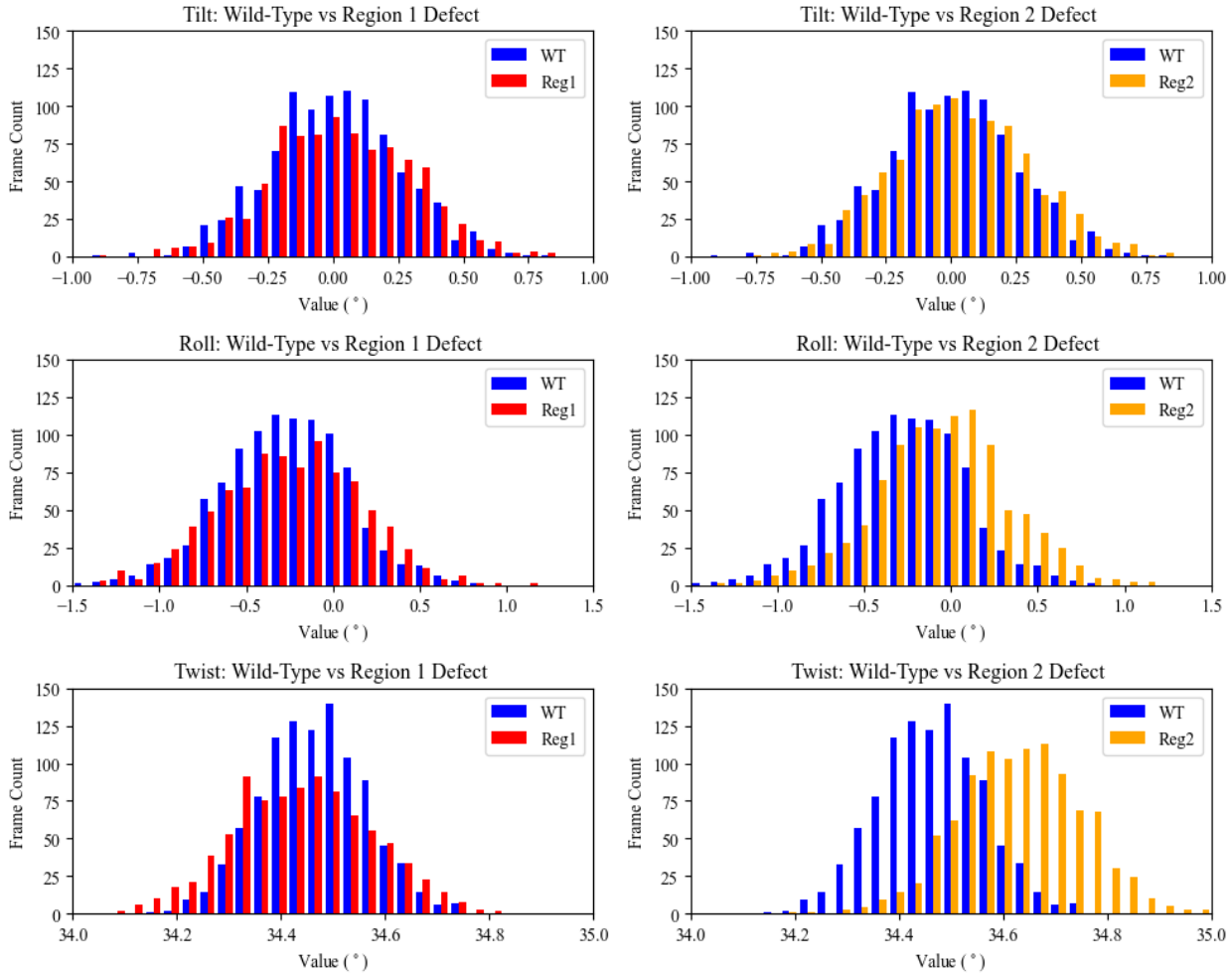

Figure 9: Population distributions of interbase rotational parameters: tilt, roll, and twist for wild-type system (WT, blue) vs region 1 defect system (Reg1, red) and for wild-type system (WT, blue) vs region 2 defect system (Reg2, orange). The systems do not include in their analysis the 40 base pairs associated with tail regions.

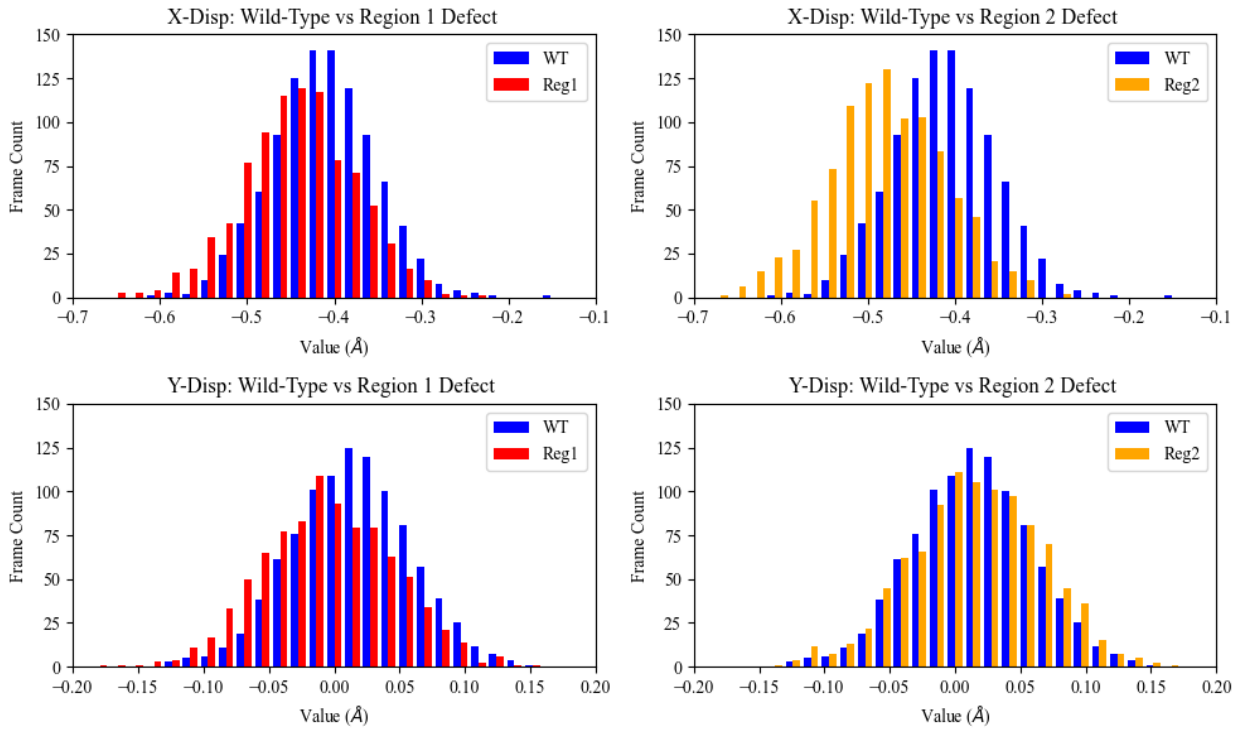

Figure 10: Population distributions of base-axis translational parameters (X- and Y-displacement) for wild-type system (WT, blue) vs region 1 defect system (Reg1, red) and for wild-type system (WT, blue) vs region 2 defect system (Reg2, orange). The systems do not include in their analysis the 40 base pairs associated with tail regions.

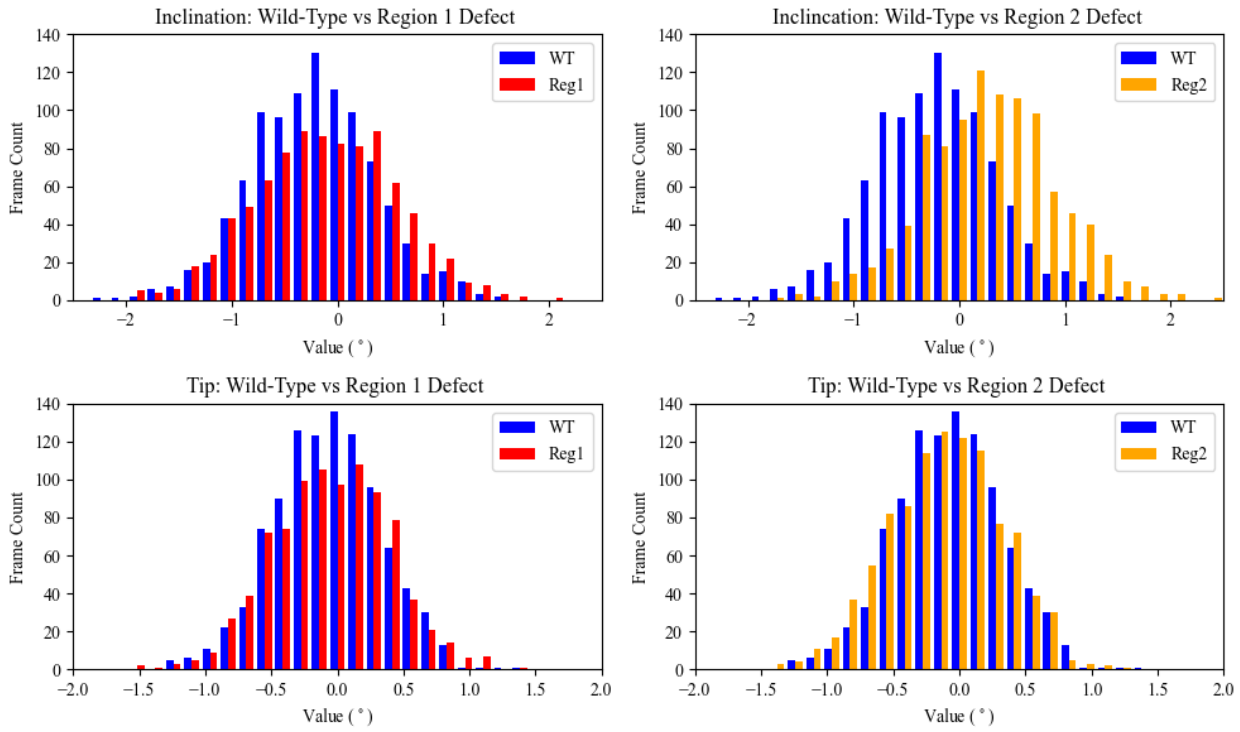

Figure 11: Population distributions of the base-axis rotational parameters (inclination and tip) for wild-type system (WT, blue) vs region 1 defect system (Reg1, red) and for wild-type system (WT, blue) vs region 2 defect system (Reg2, orange). The systems do not include in their analysis the 40 base pairs associated with tail regions.

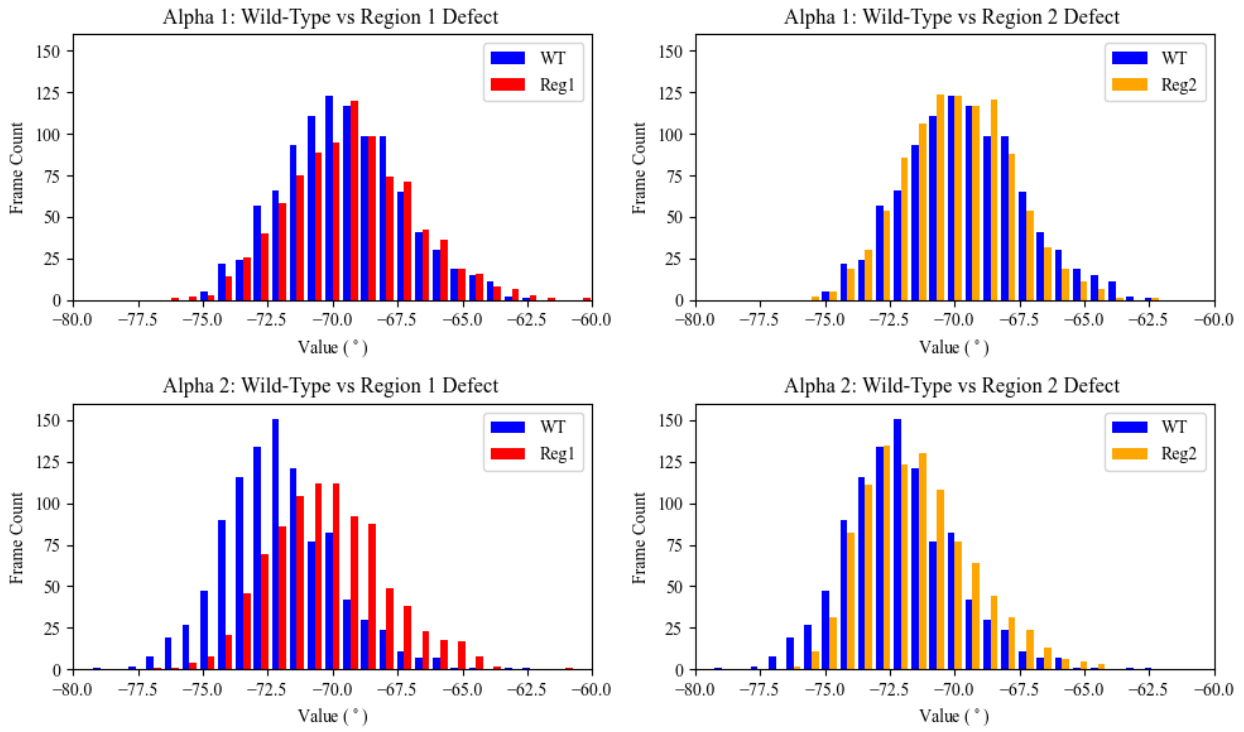

Figure 12: Population distributions of the alpha torsional angle of both DNA strands 1 and 2 for wild-type system (WT, blue) vs region 1 defect system (Reg1, red) and for wild-type system (WT, blue) vs region 2 defect system (Reg2, orange). The systems do not include in their analysis the 40 base pairs associated with tail regions.

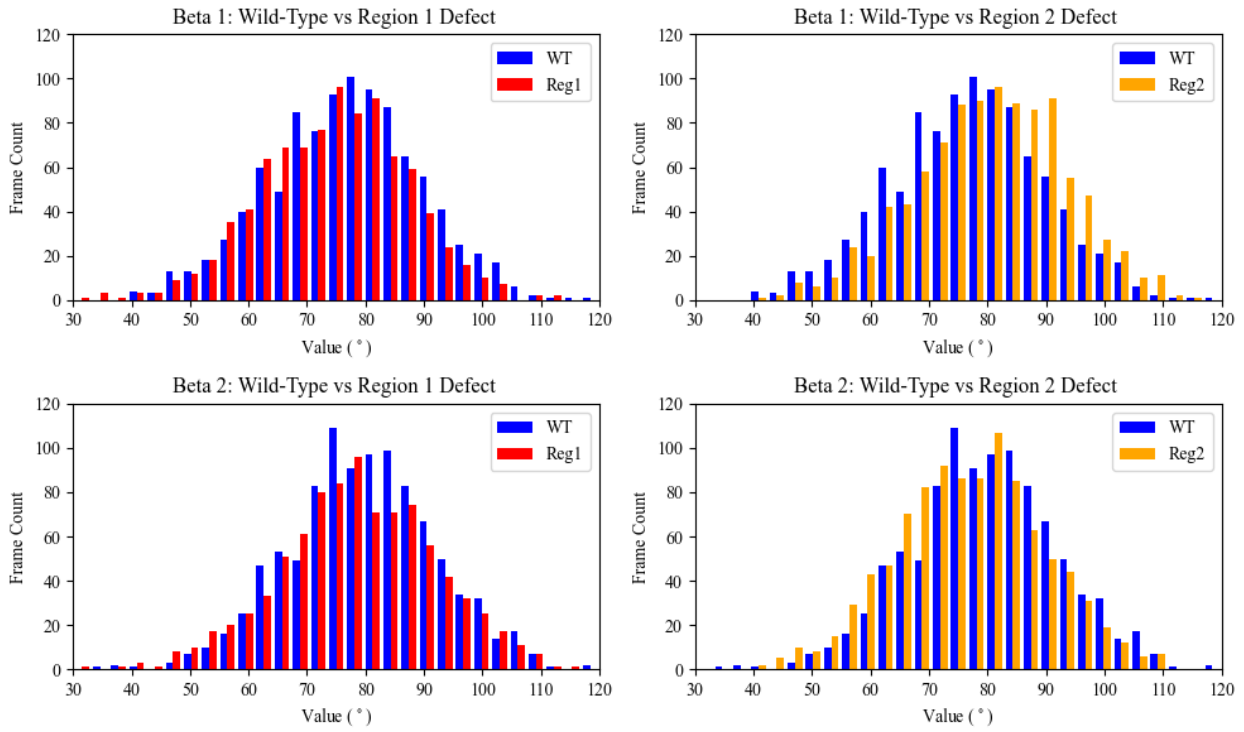

Figure 13: Population distributions of the beta torsional angle of both DNA strands 1 and 2 for wild-type system (WT, blue) vs region 1 defect system (Reg1, red) and for wild-type system (WT, blue) vs region 2 defect system (Reg2, orange). The systems do not include in their analysis the 40 base pairs associated with tail regions.

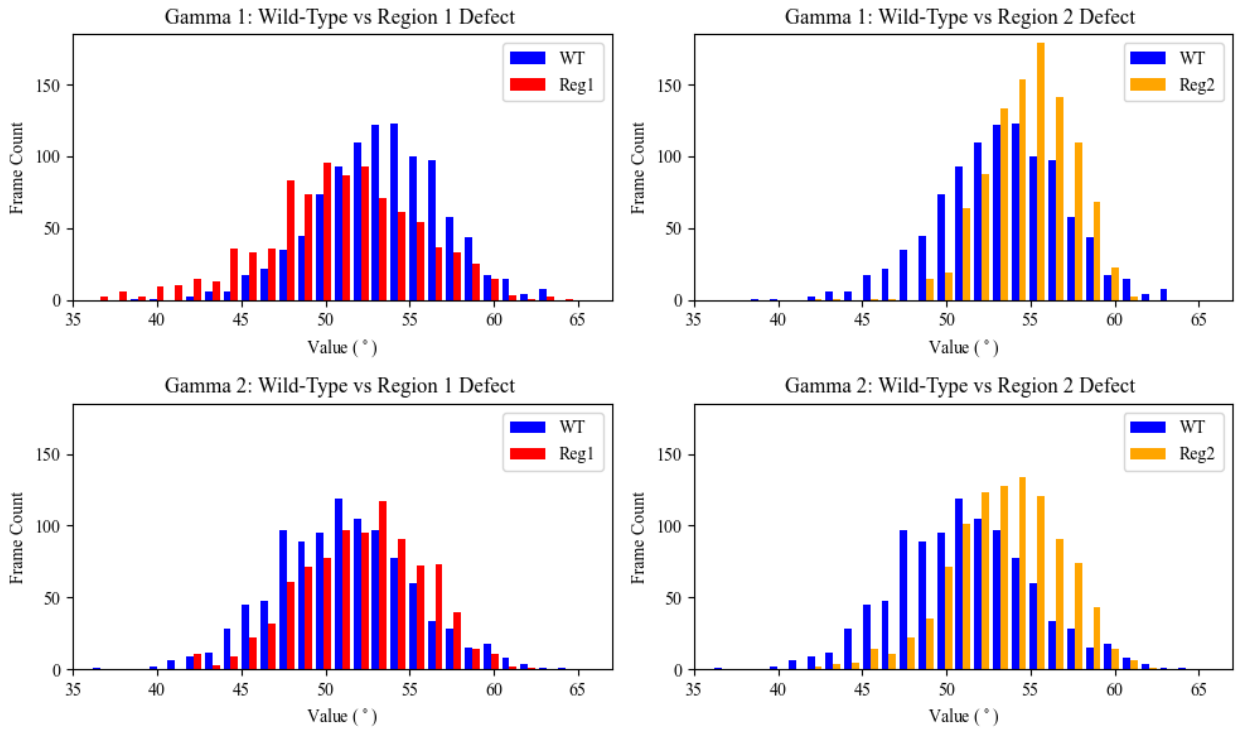

Figure 14: Population distributions of the gamma torsional angle of both DNA strands 1 and 2 for wild-type system (WT, blue) vs region 1 defect system (Reg1, red) and for wild-type system (WT, blue) vs region 2 defect system (Reg2, orange). The systems do not include in their analysis the 40 base pairs associated with tail regions.

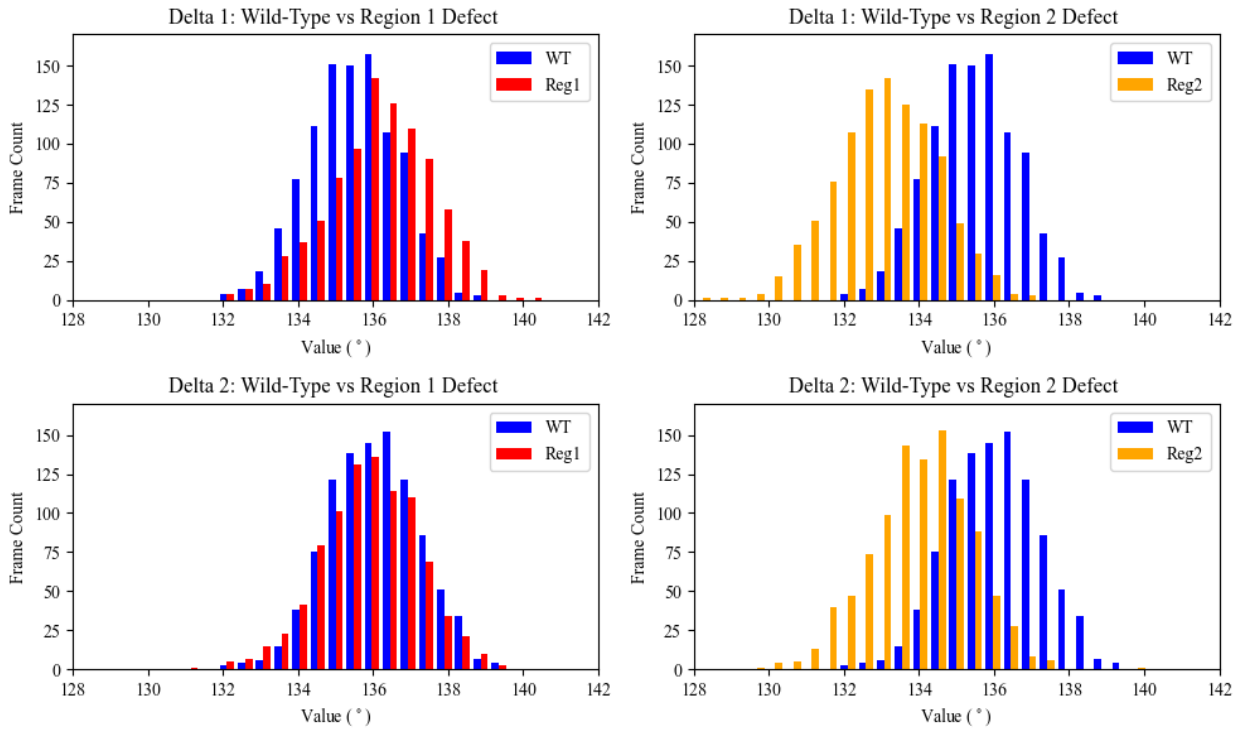

Figure 15: Population distributions of the delta torsional angle of both DNA strands 1 and 2 for wild-type system (WT, blue) vs region 1 defect system (Reg1, red) and for wild-type system (WT, blue) vs region 2 defect system (Reg2, orange). The systems do not include in their analysis the 40 base pairs associated with tail regions.

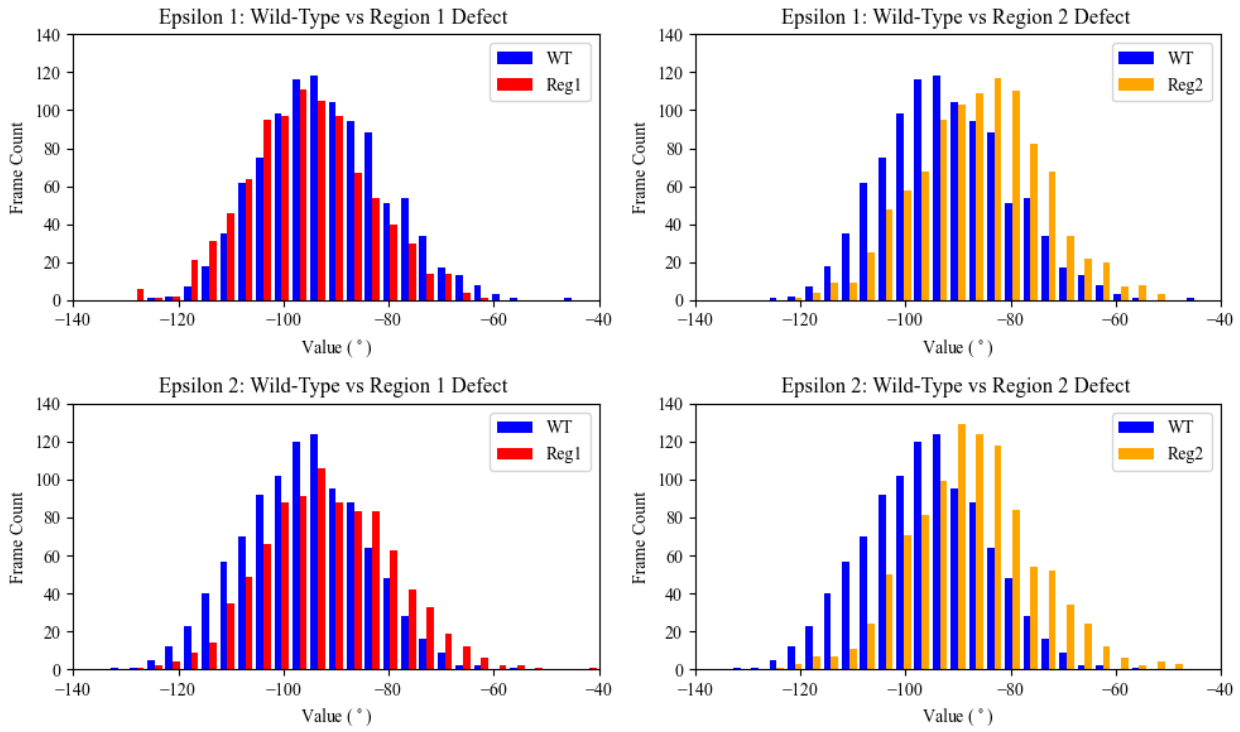

Figure 16: Population distributions of the epsilon torsional angle of both DNA strands 1 and 2 for wild-type system (WT, blue) vs region 1 defect system (Reg1, red) and for wild-type system (WT, blue) vs region 2 defect system (Reg2, orange). The systems do not include in their analysis the 40 base pairs associated with tail regions.

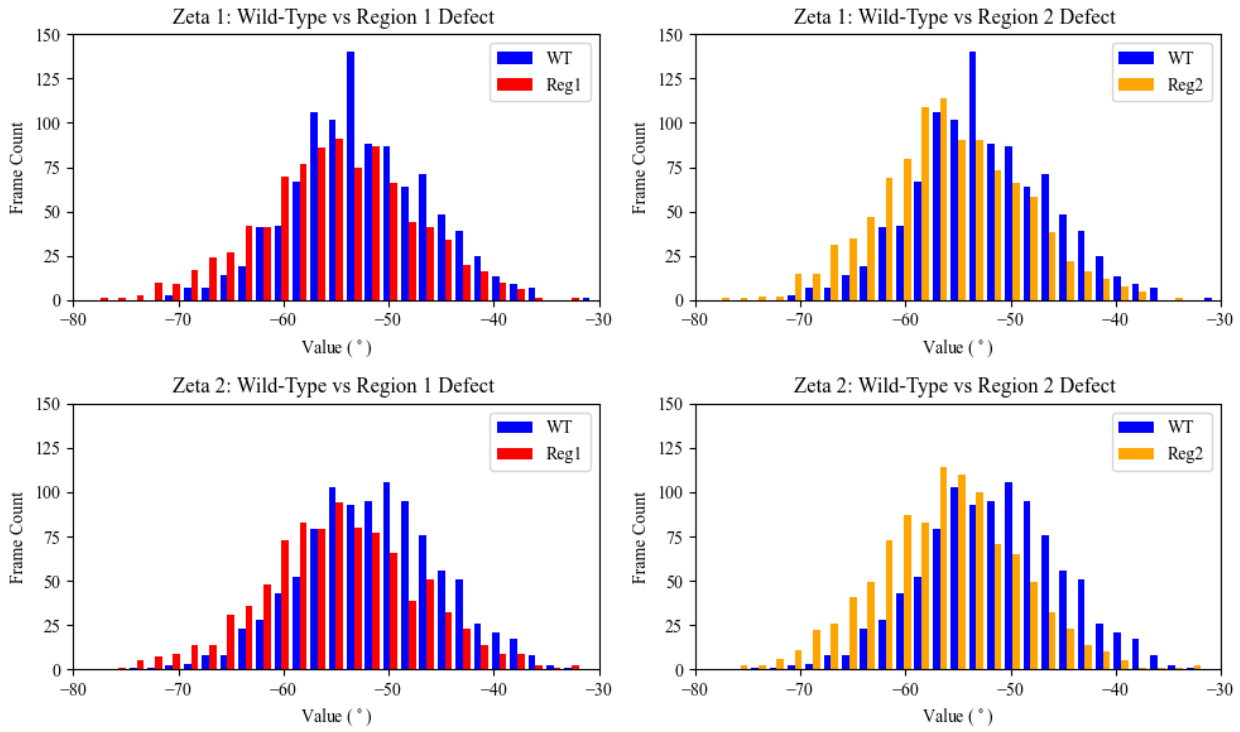

Figure 17: Population distributions of the zeta torsional angle of both DNA strands 1 and 2 for wild-type system (WT, blue) vs region 1 defect system (Reg1, red) and for wild-type system (WT, blue) vs region 2 defect system (Reg2, orange). The systems do not include in their analysis the 40 base pairs associated with tail regions.

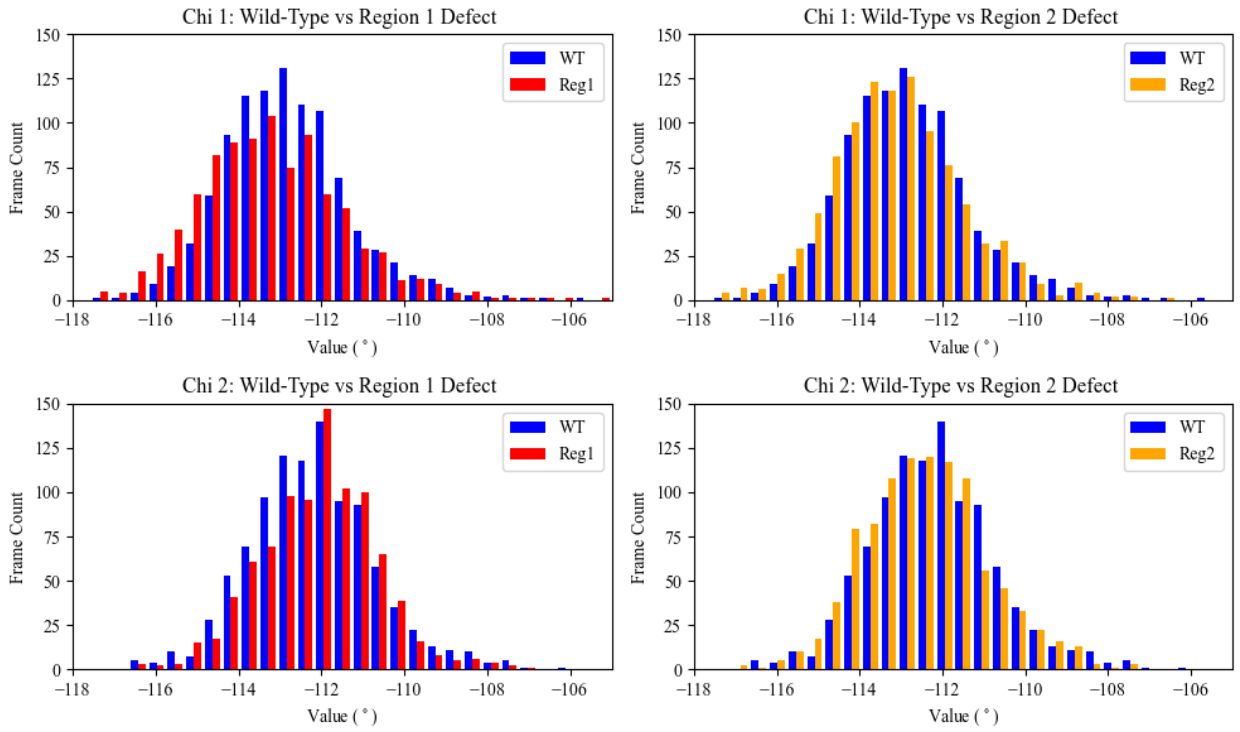

Figure 18: Population distributions of the chi torsional angle of both DNA strands 1 and 2 for wild-type system (WT, blue) vs region 1 defect system (Reg1, red) and for wild-type system (WT, blue) vs region 2 defect system (Reg2, orange). The systems do not include in their analysis the 40 base pairs associated with tail regions.

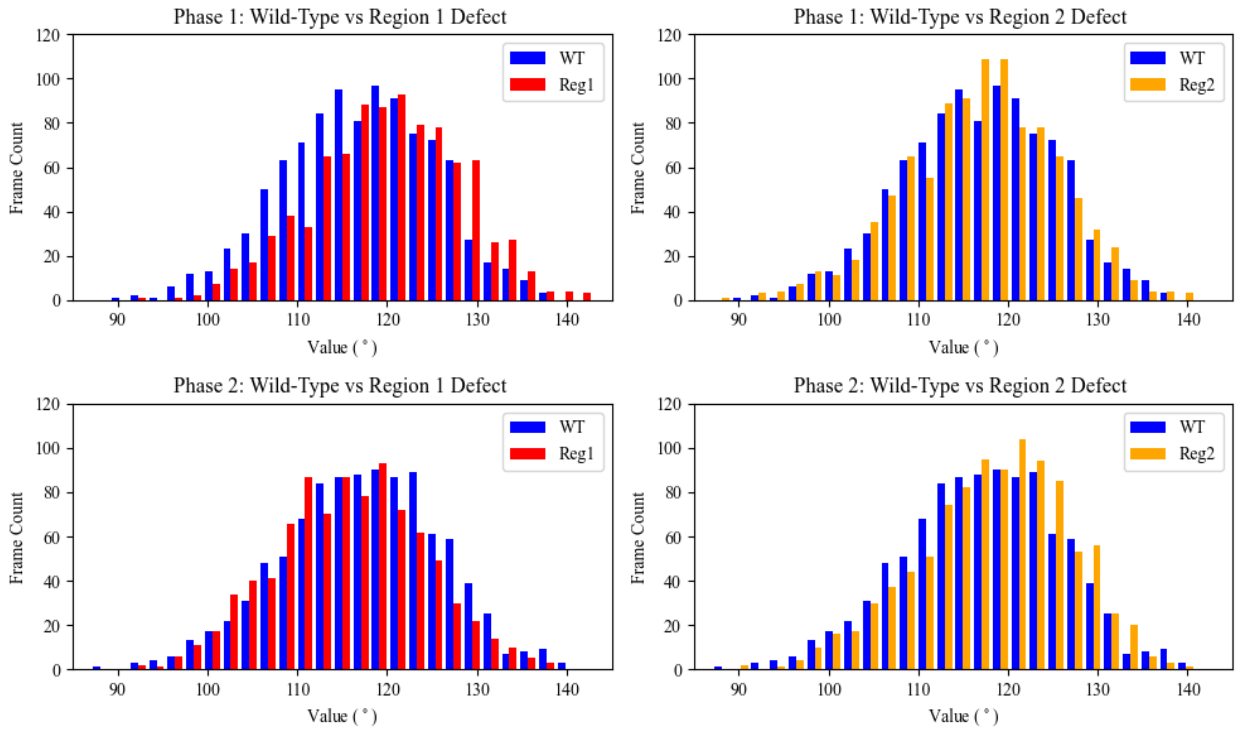

Figure 19: Population distributions of the sugar pucker phase angle of both DNA strands 1 and 2 for wild-type system (WT, blue) vs region 1 defect system (Reg1, red) and for wild-type system (WT, blue) vs region 2 defect system (Reg2, orange). The systems do not include in their analysis the 40 base pairs associated with tail regions.

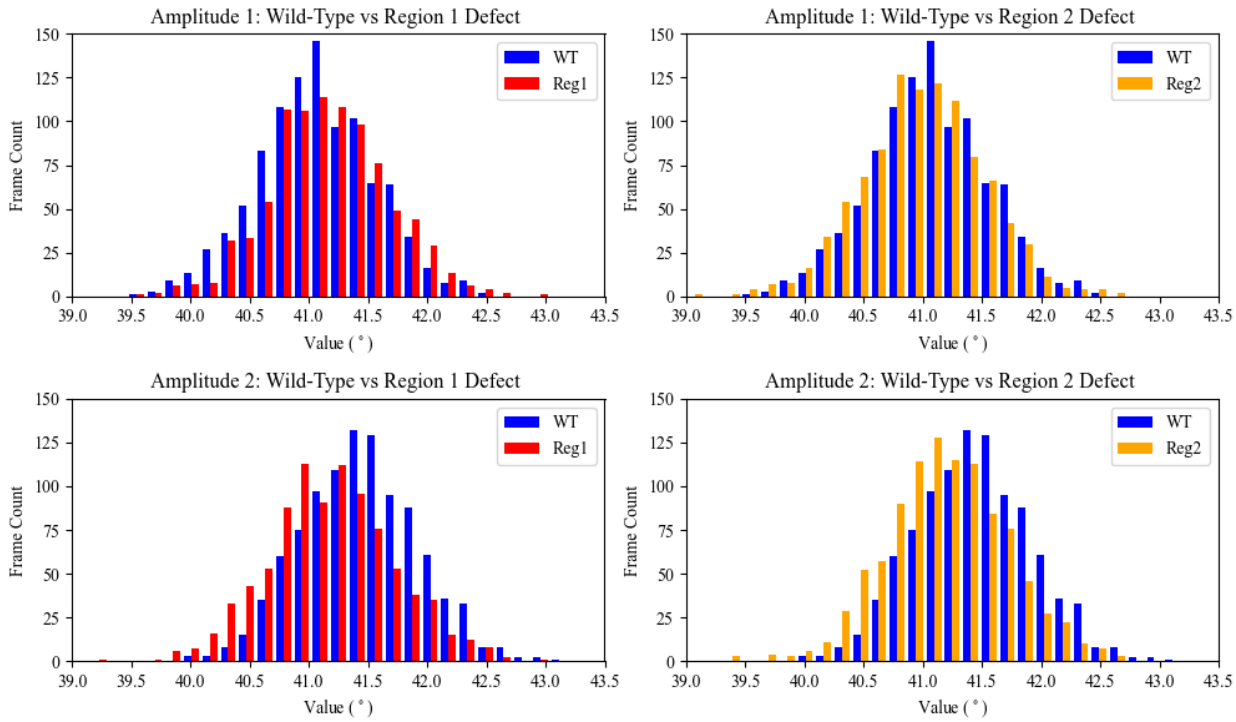

Figure 20: Population distributions of the sugar pucker amplitude of both DNA strands 1 and 2 for wild-type system (WT, blue) vs region 1 defect system (Reg1, red) and for wild-type system (WT, blue) vs region 2 defect system (Reg2, orange). The systems do not include in their analysis the 40 base pairs associated with tail regions.

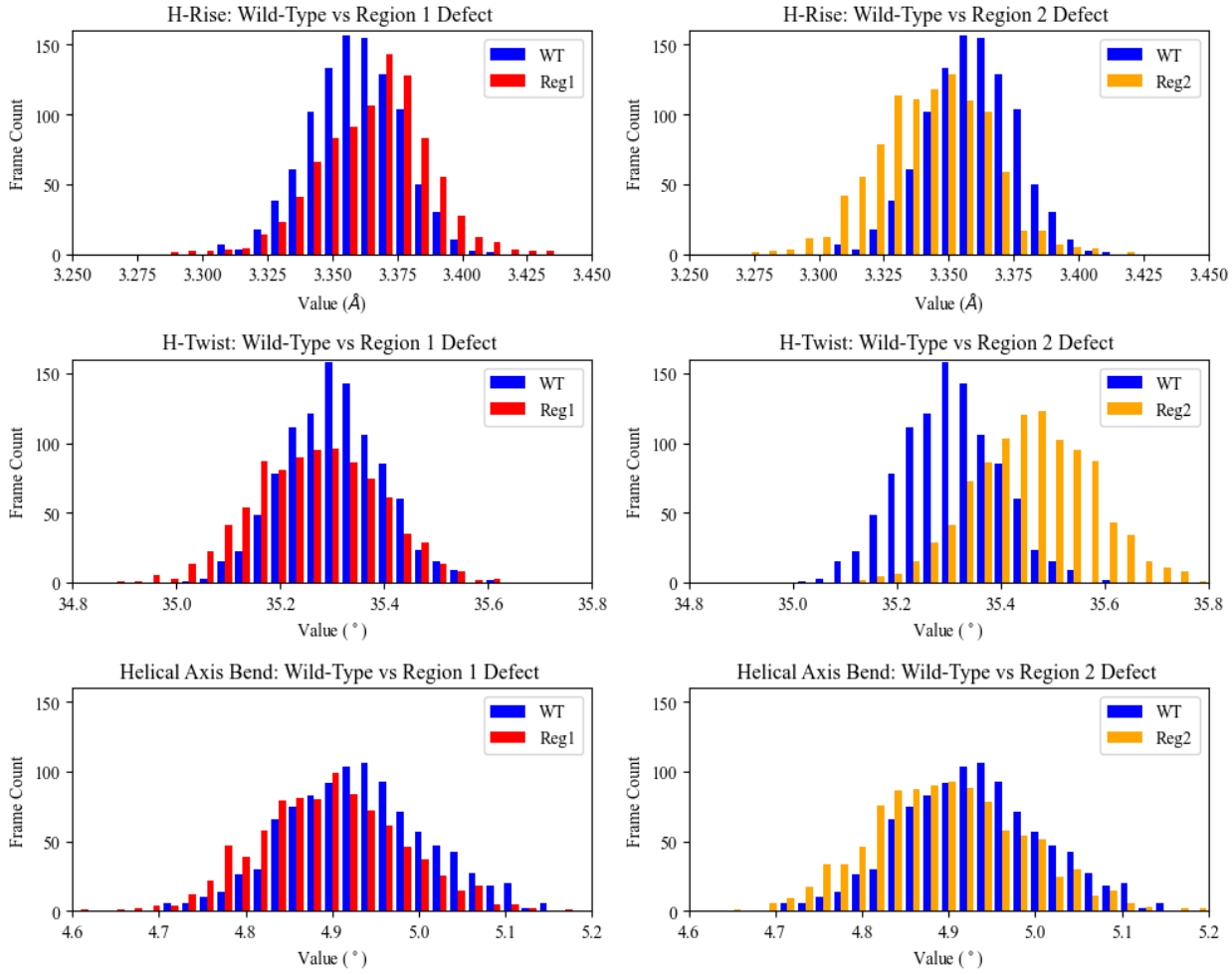

Figure 21: Population distributions of the helical rise, helical twist and the helical axis bend for wild-type system (WT, blue) vs region 1 defect system (Reg1, red) and for wild-type system (WT, blue) vs region 2 defect system (Reg2, orange). The systems do not include in their analysis the 40 base pairs associated with tail regions.

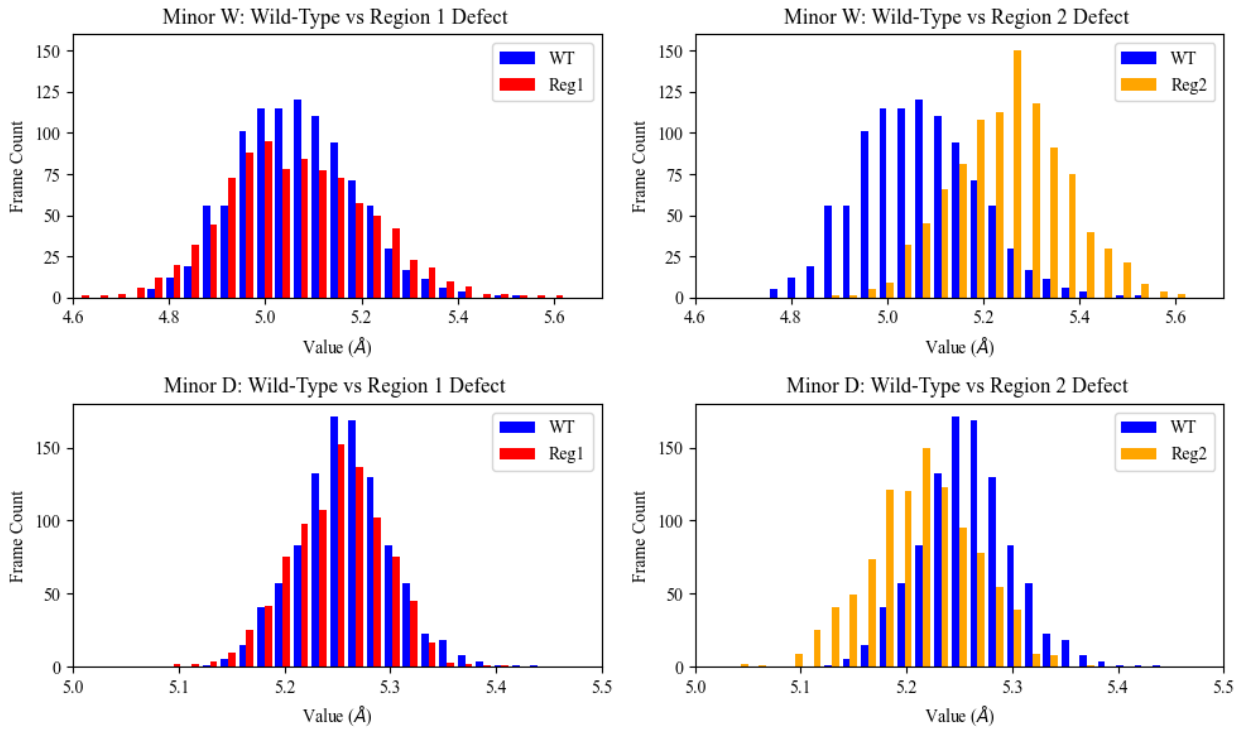

Figure 22: Population distributions of the minor groove width and depth for wild-type system (WT, blue) vs region 1 defect system (Reg1, red) and for wild-type system (WT, blue) vs region 2 defect system (Reg2, orange). The systems do not include in their analysis the 40 base pairs associated with tail regions.

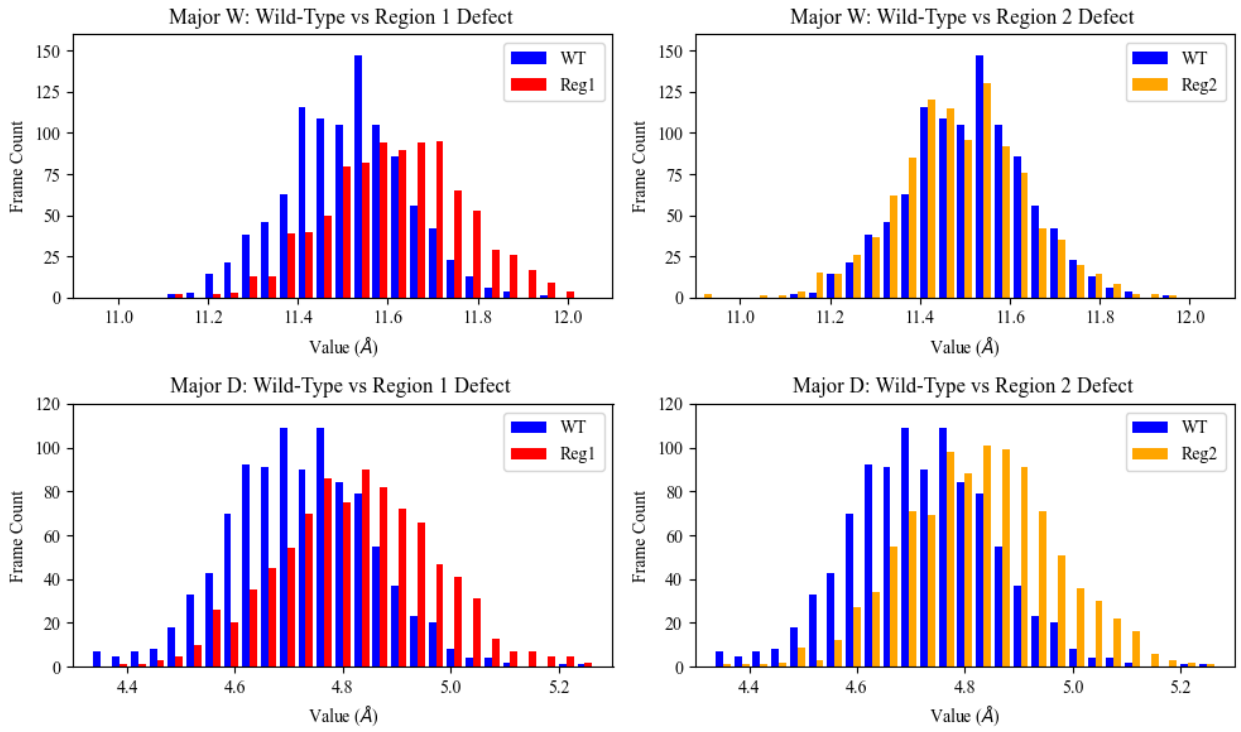

Figure 23: Population distributions of the major groove width and depth for wild-type system (WT, blue) vs region 1 defect system (Reg1, red) and for wild-type system (WT, blue) vs region 2 defect system (Reg2, orange). The systems do not include in their analysis the 40 base pairs associated with tail regions.

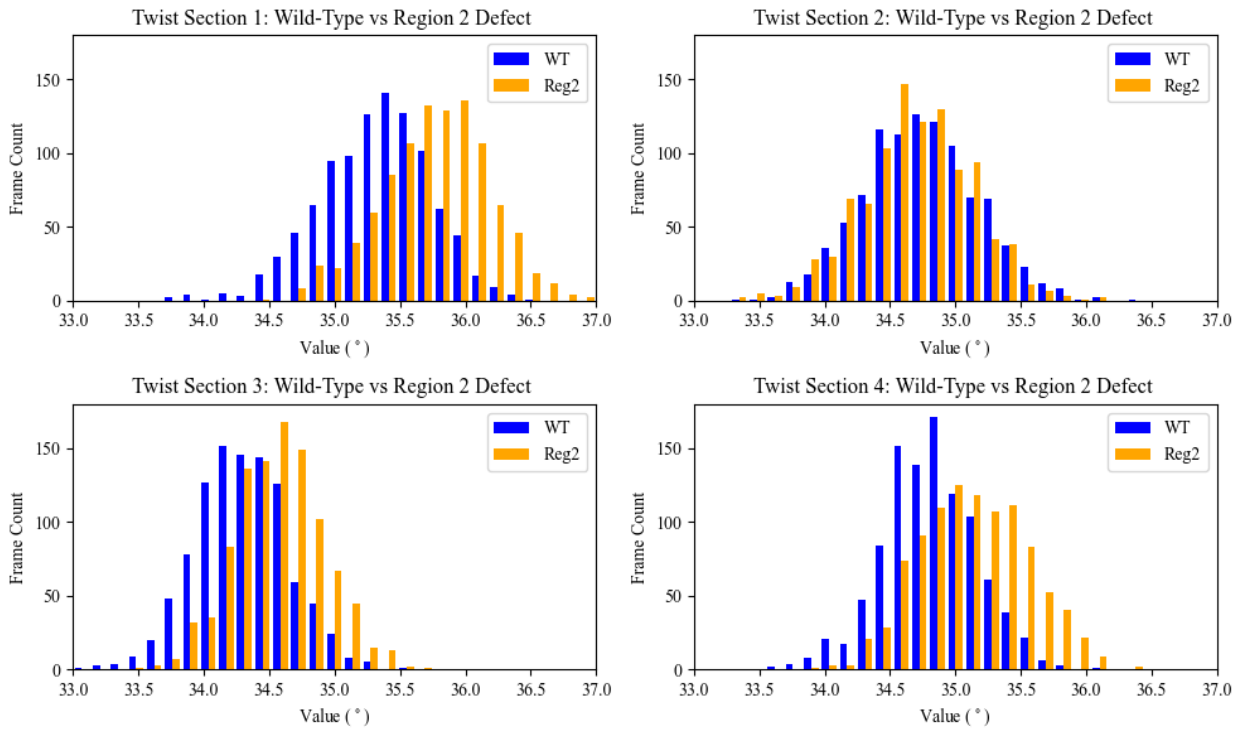

Figure 24: Population distributions of the twist parameter by NCP section for wild-type system (WT, blue) vs region 2 defect system (Reg2, orange).

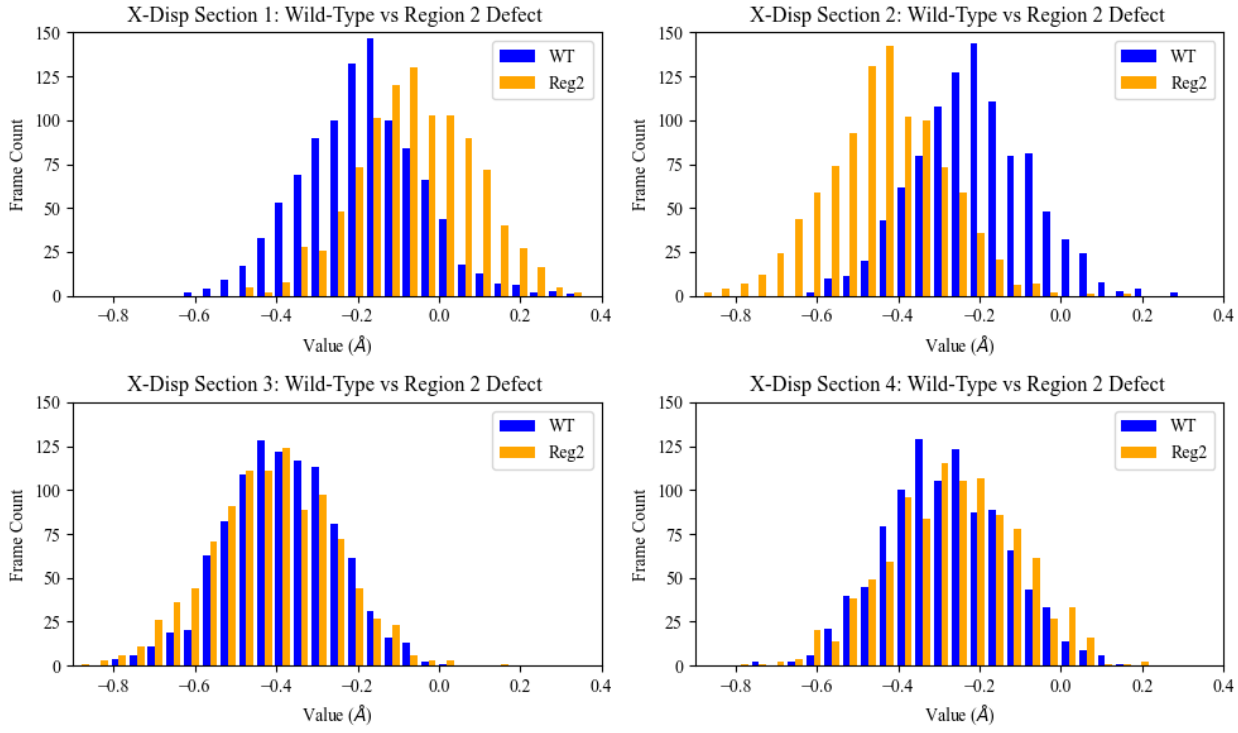

Figure 25: Population distributions of the x-displacement parameter by NCP section for wild-type system (WT, blue) vs region 2 defect system (Reg2, orange).

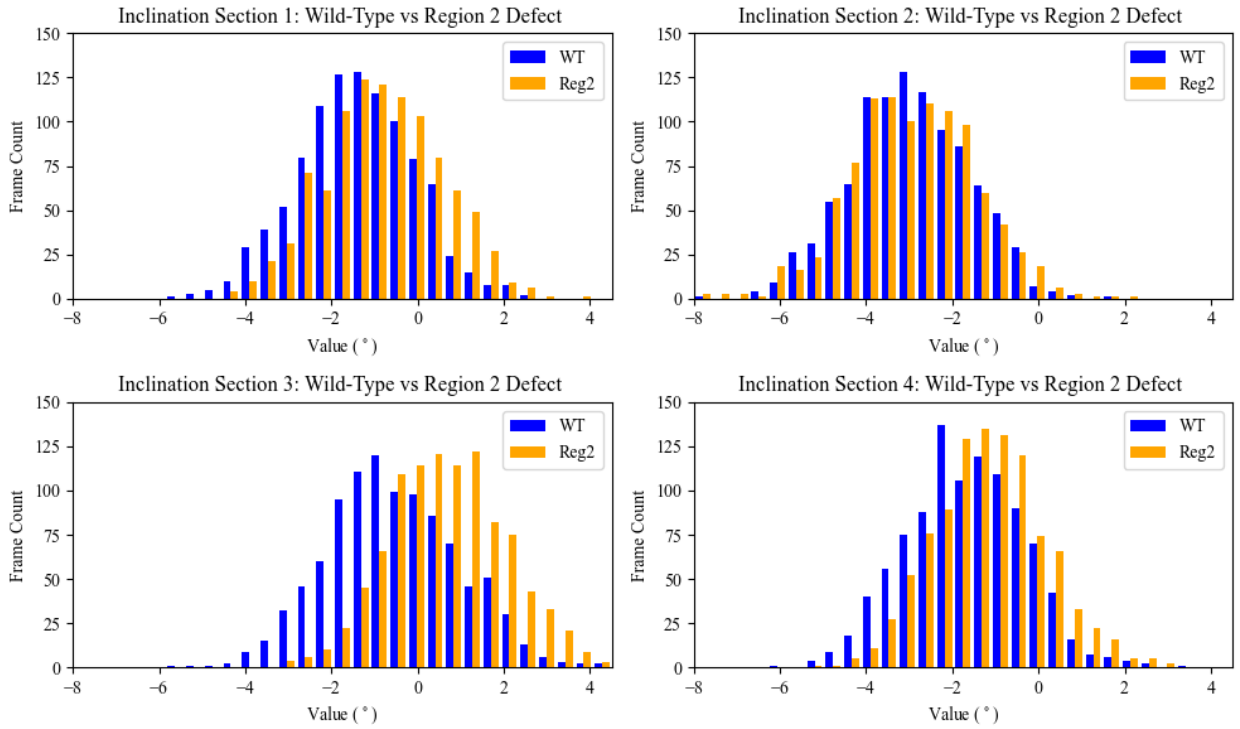

Figure 26: Population distributions of the inclination parameter by NCP section for wild-type system (WT, blue) vs region 2 defect system (Reg2, orange).

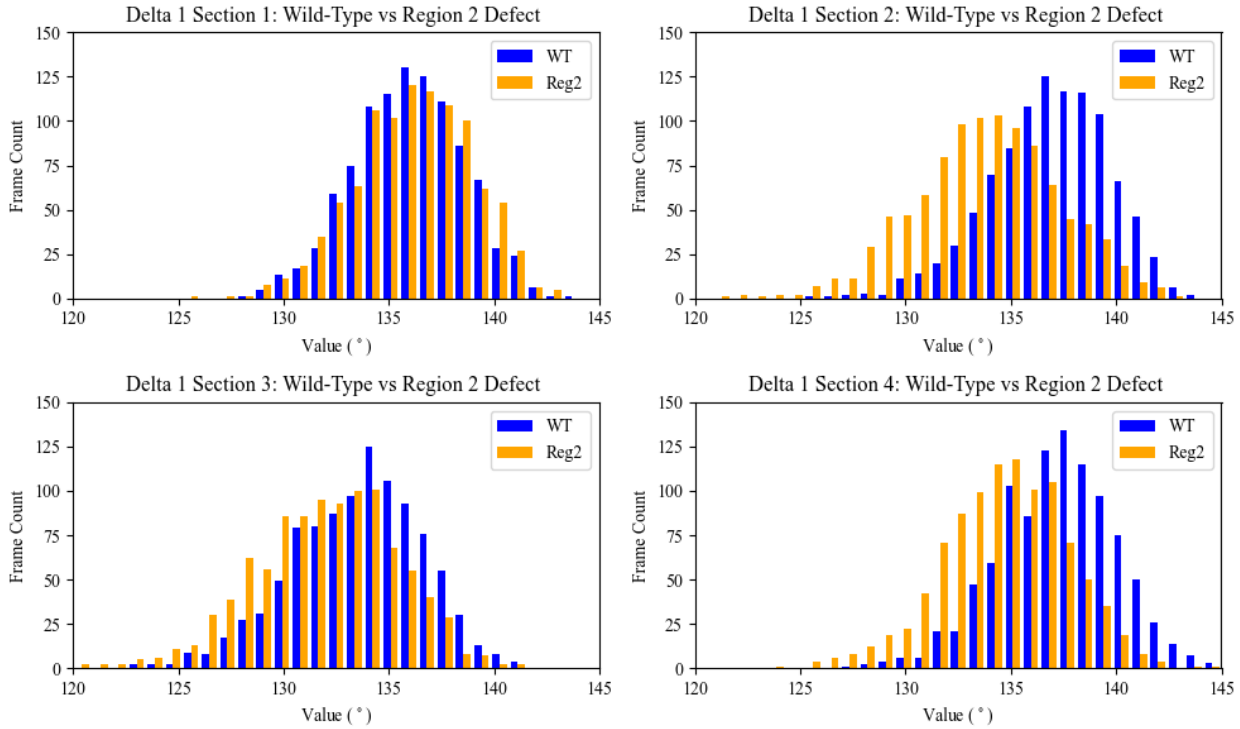

Figure 27: Population distributions of the delta torsional angle on strand 1 by NCP section for wild-type system (WT, blue) vs region 2 defect system (Reg2, orange).

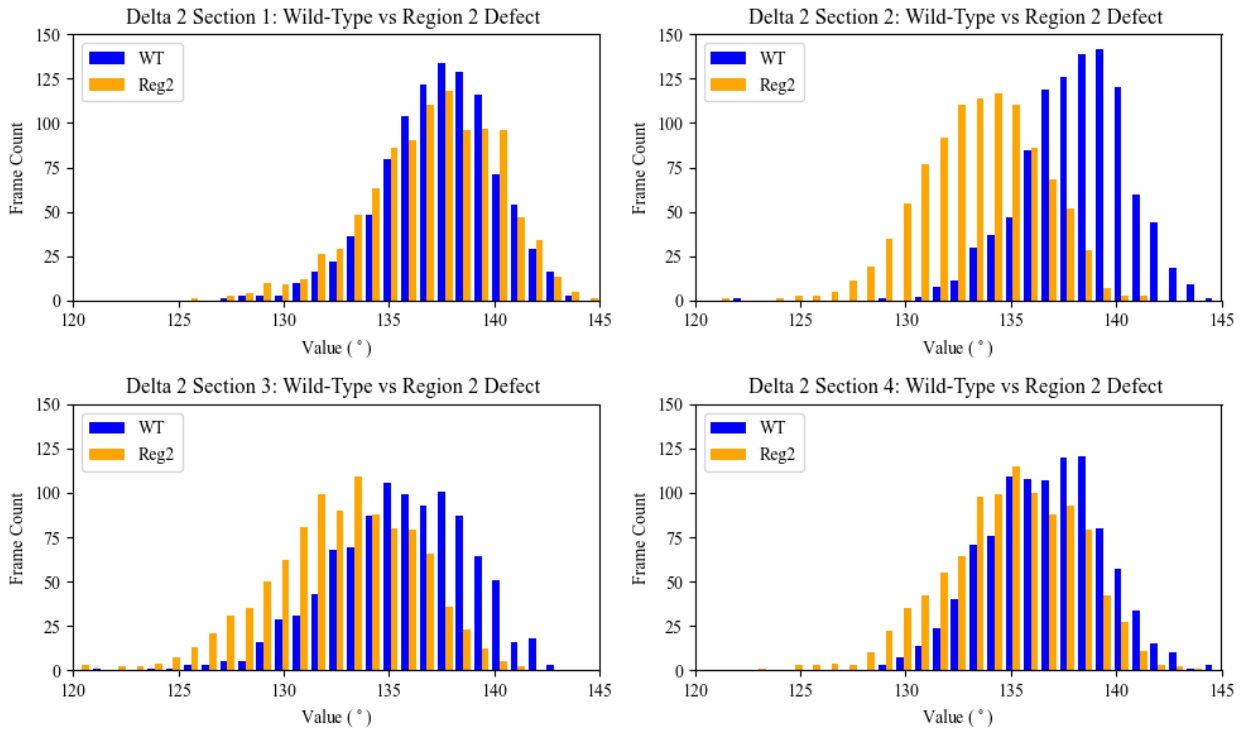

Figure 28: Population distributions of the delta torsional angle on strand 2 by NCP section for wild-type system (WT, blue) vs region 2 defect system (Reg2, orange).

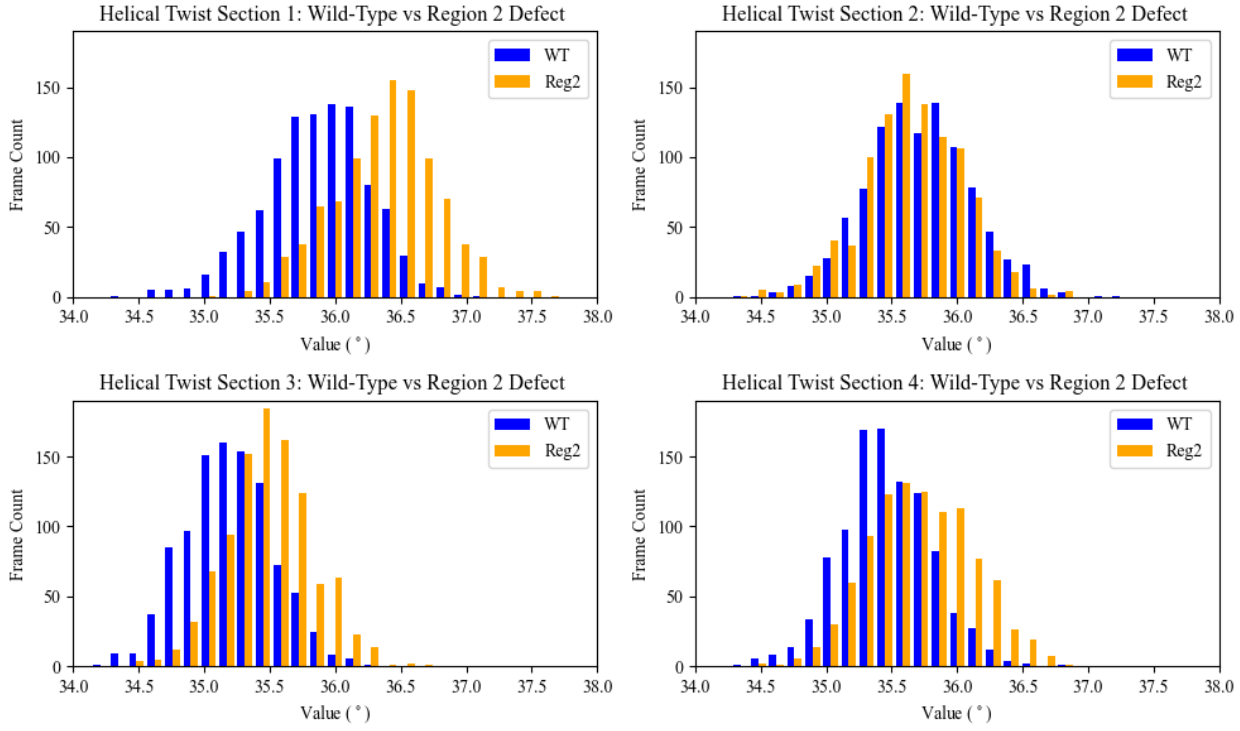

Figure 29: Population distributions of the helical twist parameter by NCP section for wild-type system (WT, blue) vs region 2 defect system (Reg2, orange).

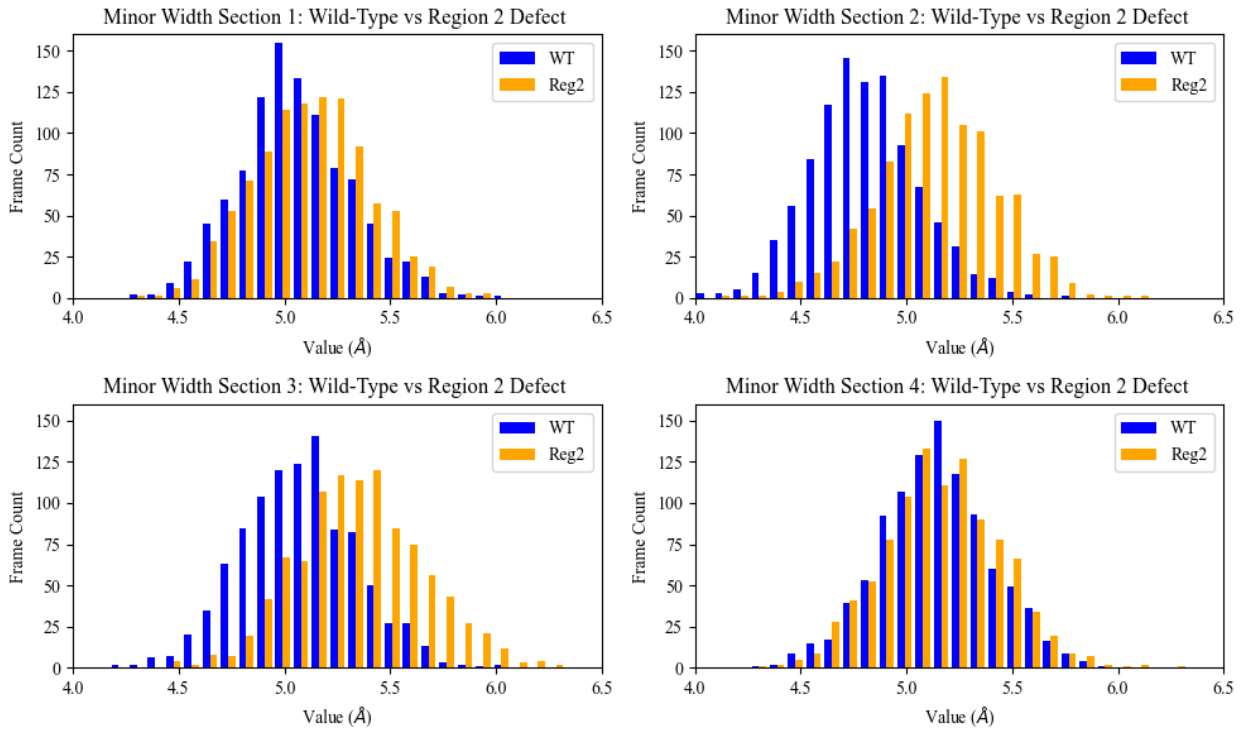

Figure 30: Population distributions of the minor groove width by NCP section for wild-type system (WT, blue) vs region 2 defect system (Reg2, orange).

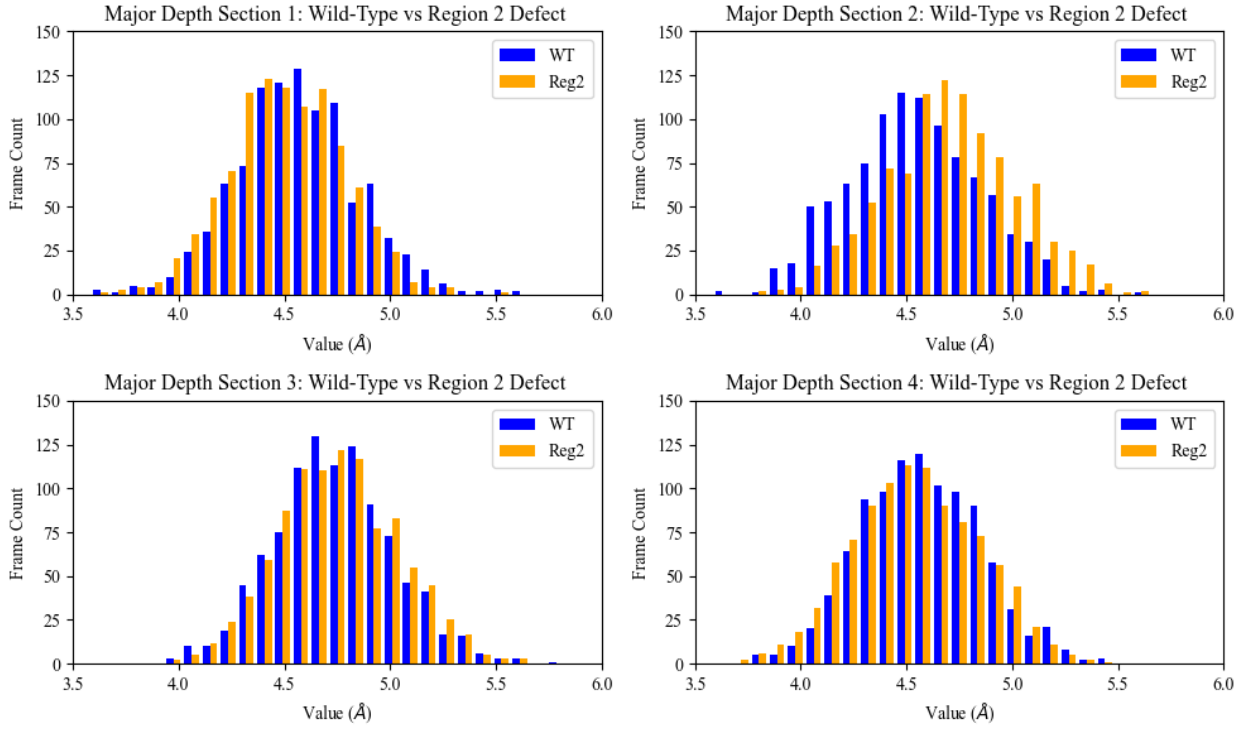

Figure 31: Population distributions of the major groove depth by NCP section for wild-type system (WT, blue) vs region 2 defect system (Reg2, orange).

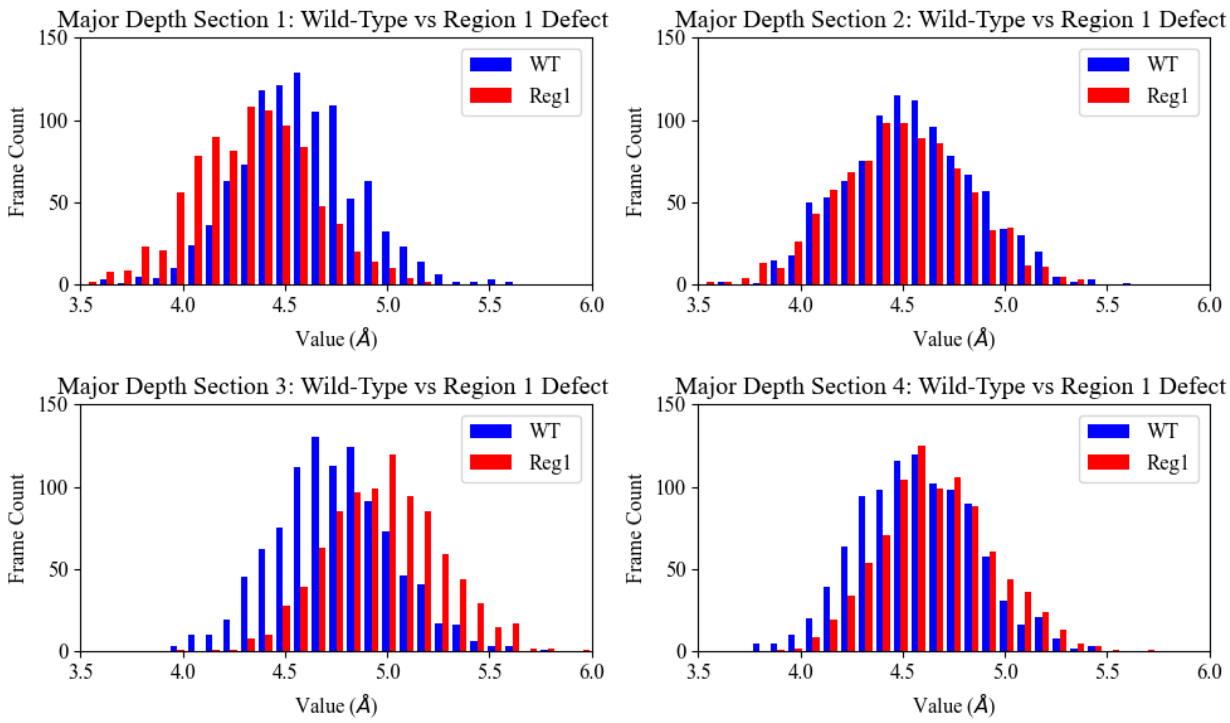

Figure 32: Population distributions of the major groove depth by NCP section for wild-type system (WT, blue) vs region 1 defect system (Reg1, red).

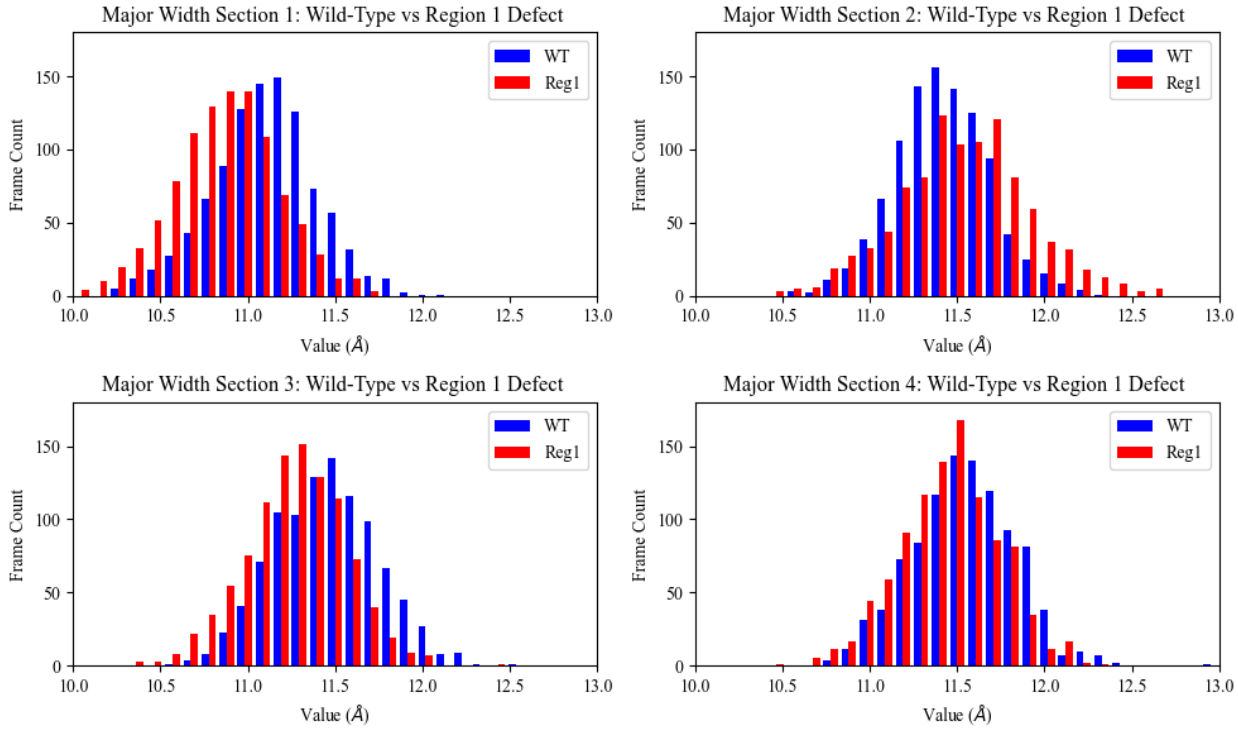

Figure 33: Population distributions of the major groove width by NCP section for wild-type system (WT, blue) vs region 1 defect system (Reg1, red).

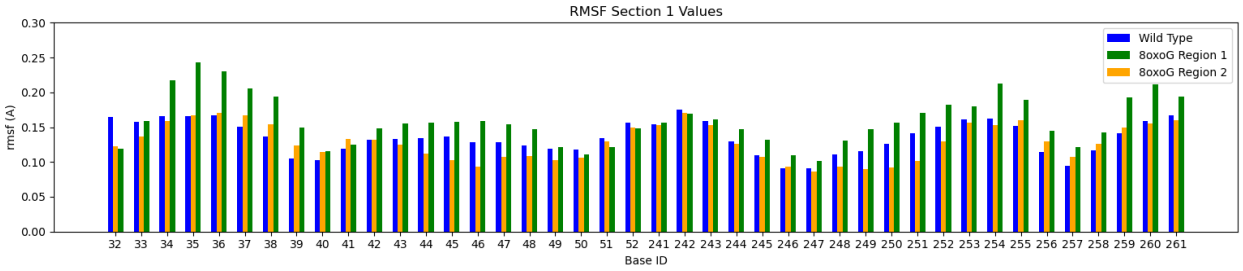

Figure 34: RMSF evaluation of section 1 bases for wild-type system (blue) vs region 1 defect system (green) and vs region 2 defect system (orange).

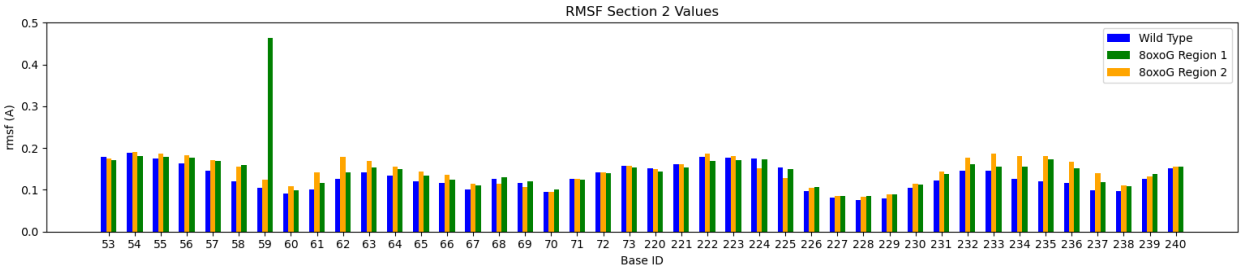

Figure 35: RMSF evaluation of section 2 bases for wild-type system (blue) vs region 1 defect system (green) and vs region 2 defect system (orange).Base number 59 of region 1 is the defect base.

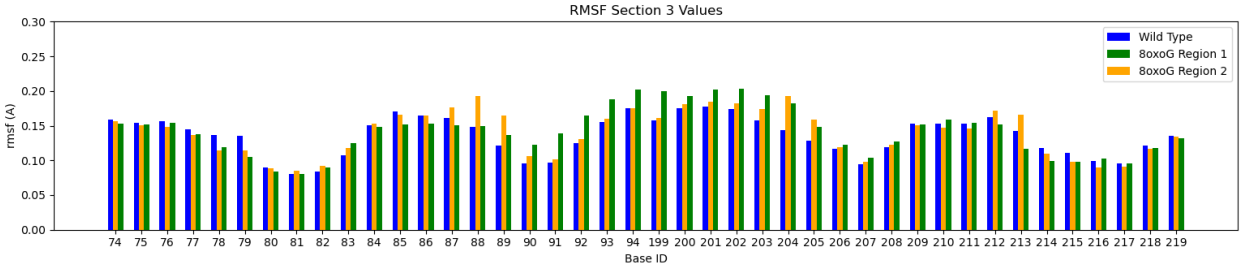

Figure 36: RMSF evaluation of section 3 bases for wild-type system (blue) vs region 1 defect system (green) and vs region 2 defect system (orange).Base number 205 of region 2 is the defect base.

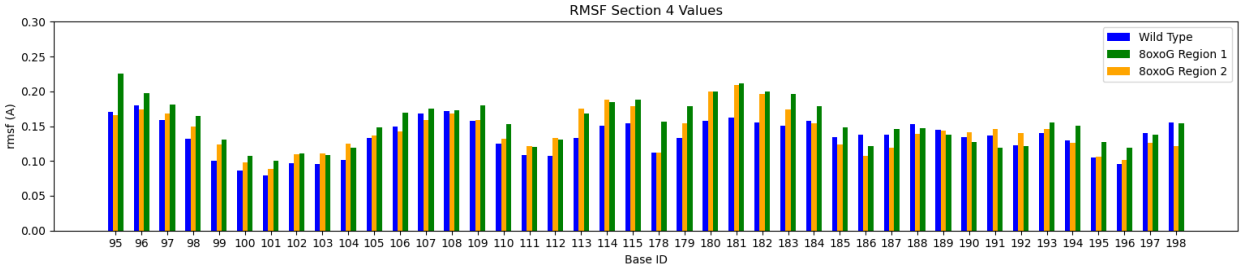

Figure 37: RMSF evaluation of section 4 bases for wild-type system (blue) vs region 1 defect system (green) and vs region 2 defect system (orange).

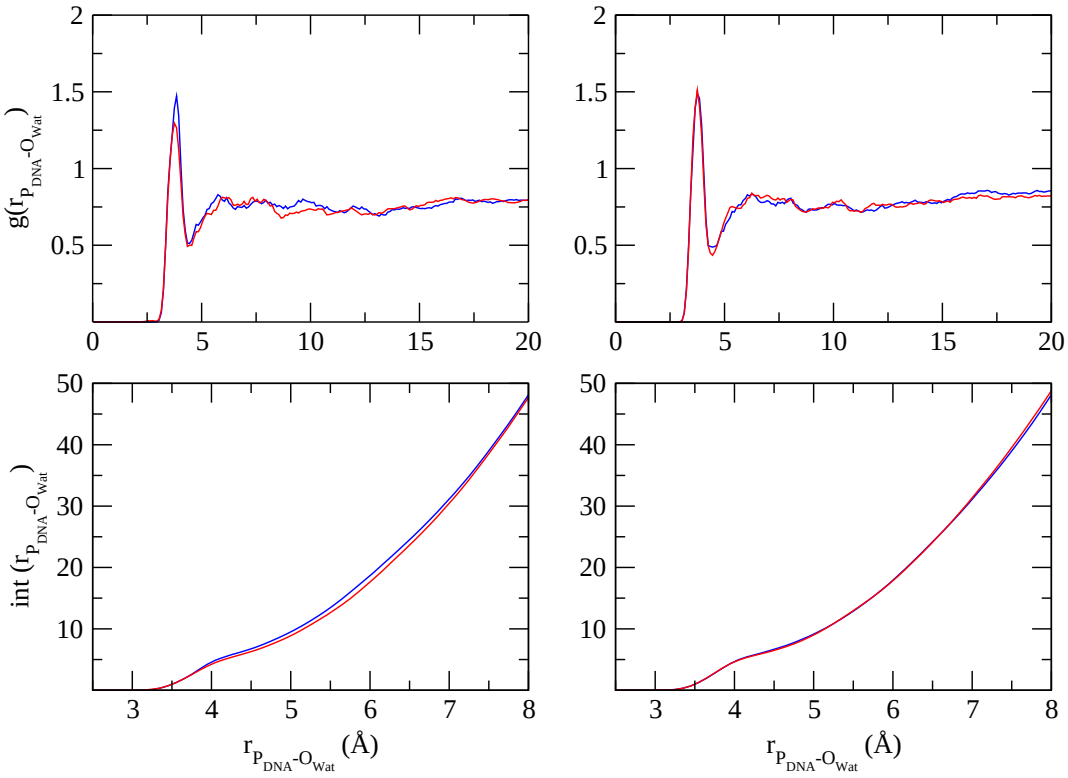

Figure 38: QM DNA-water radial distribution functions g($r_{P-O_{wat}}$), (top) and integrals (bottom) for the P and O_{wat} atoms, for the reduced state (blue colour) and oxidized state (red colour) of the native (left) and defect system (right) of **region 1**.

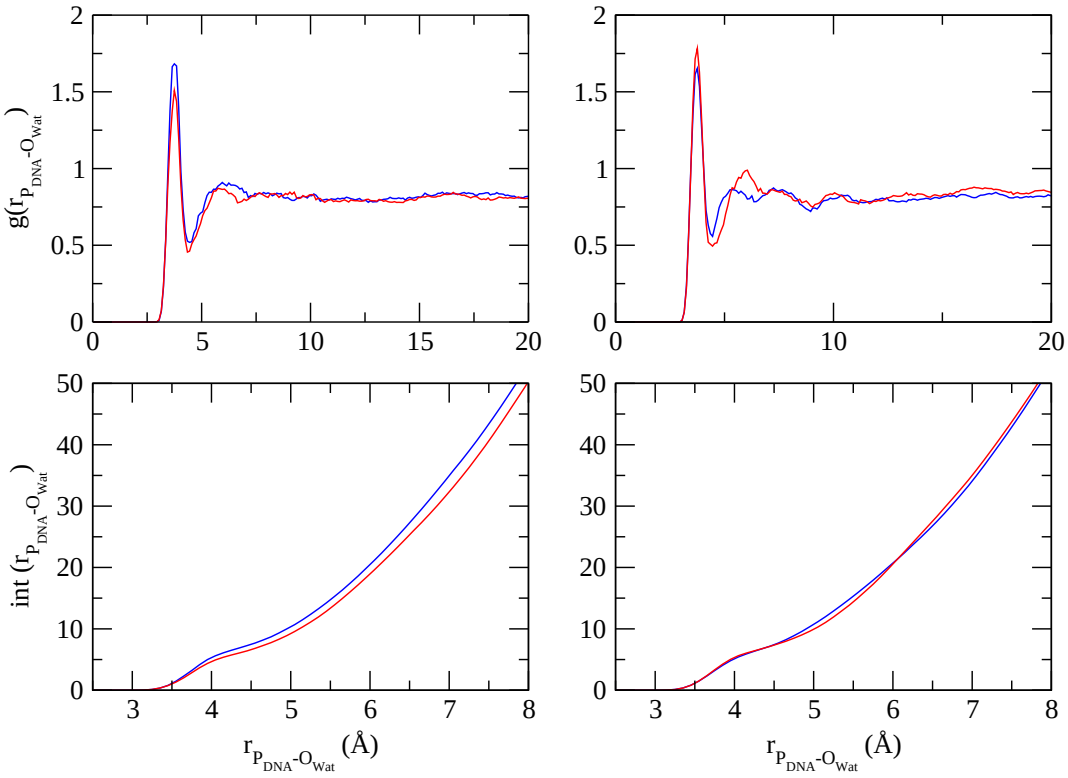

Figure 39: QM DNA-water radial distribution functions g($r_{P-O_{wat}}$), (top) and integrals (bottom) for the P and O_{wat} atoms, for the reduced state (blue colour) and oxidized state (red colour) of the native (left) and defect system (right) of **region 2**.

Author Contributions

† Murat Kılıç and Polydefkis Diamantis contributed equally to the presented work and the preparation of this manuscript.